

# On the formation of hot Neptunes and super-Earths

D. S. McNeil<sup>1\*</sup> and R. P. Nelson<sup>1</sup>

<sup>1</sup>*Astronomy Unit, School of Mathematical Sciences, Queen Mary University of London, Mile End Road, London, UK E1 4NS*

Accepted 2009 September 30. Received 2009 September 7; in original form 2009 June 22

## ABSTRACT

The discovery of short-period Neptune-mass objects, now including the remarkable system HD69830 Lovis et al. (2006) with three Neptune analogues, raises difficult questions about current formation models which may require a global treatment of the protoplanetary disc. Several formation scenarios have been proposed, where most combine the canonical oligarchic picture of core accretion with type I migration (e.g. Terquem & Papaloizou 2007) and planetary atmosphere physics (e.g. Alibert et al. 2006). To date, due in part to the computational challenges involved, published studies have considered only a very small number of progenitors at late times. This leaves unaddressed important questions about the global viability of the models. We seek to determine whether the most natural model – namely, taking the canonical oligarchic picture of core accretion and introducing type I migration – can succeed in forming objects of 10 Earth masses and more in the innermost parts of the disc.

This problem is investigated using both traditional semianalytic methods for modelling oligarchic growth as well as a new parallel multi-zone N-body code designed specifically for treating planetary formation problems with large dynamic range (McNeil & Nelson 2009). We find that it is extremely difficult for oligarchic tidal migration models to reproduce the observed distribution. Even under many variations of the typical parameters, including cases in which after the amount of mass in our disc is greatly increased above the standard Hayashi minimum-mass model, we form no objects of mass greater than 8 Earth masses. By comparison, it is relatively straightforward to form icy super-Earths.

We conclude that either the initial conditions of the protoplanetary discs in short-period Neptune systems were substantially different from the standard disc models we used, or there is important physics yet to be understood and included in models of the type we have presented here.

**Key words:** planetary systems: formation

## 1 INTRODUCTION

At present, there are  $\sim 19$  known extrasolar planets<sup>1</sup> with estimated masses between 0.03 and 0.12  $M_{\text{Jup}}$ , or between  $\sim 10$  and  $\sim 40 M_{\oplus}$ . With one exception – OGLE-05-169L b, at 2.8 AU – all of the planets have semimajor axes smaller than 1 AU, and so are reasonably called hot Neptunes. In fact, with only one more exception, HD69830 d, all have semimajor axes  $< 0.23$  AU. To determine whether the objects are genuine Neptunes, i.e. ice giants, and not merely very large rocky bodies better thought of as super-Earths, knowledge of the mean densities is required. Three of these objects have

known radii, and two have mean densities compatible with being a Neptune-like body. GJ436 b (Butler et al. 2004) has a density of  $\sim 1.69 \text{ g/cm}^3$  (Torres et al. 2008), and HAT-P-11 b (Bakos et al. 2009) has a density of  $\sim 1.33 \text{ g/cm}^3$ ; compare Neptune with  $1.64 \text{ g/cm}^3$ . The HD69830 system (Lovis et al. 2006) is particularly interesting. It contains three Neptune-like objects: HD69830 b at 0.0785 AU, of  $10.5 M_{\oplus}$  and eccentricity 0.1; HD69830 c at 0.186 AU, of  $12.1 M_{\oplus}$  and eccentricity 0.13; and HD69830 d at 0.63 AU, of  $18.4 M_{\oplus}$ , and eccentricity 0.07 ( $\pm 0.07$ , so a near-circular orbit is possible). The system was also reported to have a disc of warm infrared-emitting dust located between planets c and d (Beichman et al. 2005), presumably due to a collisionally active remnant asteroid belt. More recent work (Lisse et al. 2007) suggests instead that the infrared excess is due to a debris disc outside the known planets at  $\simeq 1$  AU,

\* E-mail: d.mcneil@qmul.ac.uk

<sup>1</sup> Data taken from the Extrasolar Planets Encyclopedia, Schneider, J., <http://exoplanet.eu>

probably resulting from the breakup of an asteroid. This system clearly provides a rigorous test of planet formation and migration theories.

Indeed, short-period Neptune-mass bodies have several advantages as probes of planetary origins. They are large enough to be observable, but small enough that we need not consider gravitational disc instability as a formation process. They are also large enough to undergo significant type I migration, but not so large that they can open a gap in the disc and undergo type II migration (Papaloizou & Lin 1984; Bryden et al. 1999; Crida et al. 2006). Accordingly, hot Neptunes can yield less ambiguous tests of type I migration than more massive planets which could have significantly perturbed the gas disc they were embedded in, and their existence provides strong evidence that some kind of type I migration is operating in protoplanetary discs.

Hot Neptunes are therefore useful for exploring the intersection of the classical oligarchic core accretion picture (Kokubo & Ida 1998; e.g. Chambers 2001; Thommes et al. 2003) with type I migration (Ward 1997). Two main classes of scenario exist in the literature: one which concentrates on the atmospheric gas physics, and one which concentrates on the dynamics of the protoplanetary interactions.

Alibert et al. (2006) incorporate sophisticated atmospheric physics and follow the evolution of effectively isolated cores through the disc as they grow via planetesimal accretion, migrate inwards due to type I effects, accrete gas after the accretion rate of solids drops, and finally have their atmospheric mass reduced after arriving in the short-period region by evaporation. However, the history for the HD69830 system proposed in Alibert et al. (2006) is difficult to reconcile with the oligarchic paradigm (Kokubo & Ida 1998). Their best-fitting model involves exactly three seed objects of masses  $M = 0.6 M_{\oplus}$  at semimajor axes 3 AU, 6.5 AU, and 8 AU, which migrate to small semimajor axis through a mostly pristine planetesimal disc and therefore can accrete a fair amount of material (Tanaka & Ida 1999). Where did these three progenitor objects come from? In an oligarchic framework, accretion in a narrow region – even in the presence of type I drag (see Kominami et al. 2005; McNeil et al. 2005; Daisaka et al. 2006) – results in many roughly equal-mass bodies separated by a distance of  $10 \sim 20$  Hill radii. These bodies then interact and merge in the giant-impact phase of planet formation, and consume the accessible remnant planetesimal disc. That is, if a half-Earth-mass seed can successfully form at 3 AU, there should be a large number of similar seeds of varying mass inside, each of which will accrete and migrate in similar ways. Moreover, the interior seeds are likely to have formed first. The net result is that any such inward-migrating seed should be migrating through a region highly depleted by the previous seeds, and by the time an  $0.6 M_{\oplus}$  core is formed at 3 AU much of the interior disc should have gone to completion, and possibly formed its own planets (Chambers 2008). There is no obvious mechanism to suppress embryo growth everywhere in the disc except at three specific locations. An additional problem is that simulations have demonstrated that cores migrating through a planetesimal swarm are unable to grow at the rate prescribed by the Alibert et al. (2006) model. In the presence of gas drag, mean motion resonances cause the majority of the interior planetesimals to be shepherded rather than being accreted, resulting in planets whose masses are too

low, and in the wrong ratio, compared to those observed in the HD69830 system (Payne et al. 2009).

Though not aiming at HD69830 in particular, Terquem & Papaloizou (2007) study the formation of hot super-Earths and Neptunes by following the evolution of 10–25 planets of  $0.1$  or  $1 M_{\oplus}$  placed interior to 2 AU under type I drag, include tidal interactions with the star, and use an inner cavity in the gas disc at  $\sim 0.05$  AU. For various disc parameters, they succeed in making several objects of mass  $\geq 8 M_{\oplus}$ , with a maximum of  $12 M_{\oplus}$ . They find that the typical result has between 2–5 planets, usually on near-commensurable orbits (with strict commensurability often being broken by tidal circularization). It is not clear whether this will scale up to larger masses, as they performed only one run with total mass larger than  $12 M_{\oplus}$  (namely  $25 M_{\oplus}$ ), and so an HD69830-like system would not appear in their results even if the model would have succeeded in producing them. Very little material was lost from their runs, suggesting it might be possible. However, their initial configurations are difficult to reconcile with an oligarchic migration process.

Scenarios involving oligarchic formation and type I migration do not exhaust the possible formation histories of the low-mass hot exoplanet population, although they are arguably the most natural. Raymond et al. (2008) surveys several other proposed possibilities (for the terrestrial-mass regime): in situ formation; shepherding by migrating giant planets or secular resonance sweeping; tidal circularization; and photoevaporation of giant planets. We will concentrate instead on the simplest oligarchic type I migration picture, which should have more success self-consistently generating an icy planet population, and attempt to determine whether the fiducial models can reproduce the observed distribution of hot Neptunes. If they can, all the better; if they cannot, then the specifics of their failure may point in the direction of a solution and help us choose between the various possibilities on offer.

To understand how short-period Neptunes are formed, we need to move toward self-consistent global N-body models such as those which have proved useful in understanding the formation of the terrestrial planets and the outer solar system. One problem presents itself immediately: the short-period exoplanet problem has a formation time to dynamical time ratio  $\sim 30$  times larger than the equivalent terrestrial formation problem, and  $\sim 1000$  times that of the equivalent Jovian core formation problem. The lifetime of the gas disc (with a probable upper limit of  $\sim 6$  Myr) is a common reference time-scale for each problem, as gas giants must form while there is still gas for them to accrete, and even ice giants which attain short-period orbits must have migrated while there is gas present. However, the characteristic orbital periods for each formation problem vary from 0.01 yr at 0.05 AU to 0.35 yr at 0.5 AU to 11 yr at 5.0 AU. (Indeed, 0.01 yr is optimistic, as many exoplanets are closer to their parent stars than 0.05 AU.) Since most state-of-the-art planetary N-body codes require the integration timestep to be some small fraction of the orbital period of the innermost object, preserving the same wall-clock run times that researchers have become accustomed to would usually require reducing the number of planetesimals in a simulation by orders of magnitude, producing an unacceptable decrease in resolution.

It is extremely unlikely that this difficulty can be elim-

inated entirely, as it is a consequence of the strong dependence of orbital period on semimajor axis in the Kepler problem. That said, the challenge can be managed to some extent by taking advantage of the scale separation caused by the troublesome dynamic range. The standard approaches use a common drift timestep for all particles (and therefore “over-integrate” the more distant objects) and compute the (non-encountering) forces between the particles at the same frequency, both of which involve far more computation on the distant, slow-moving objects than is necessary to preserve qualitatively accurate dynamics. In McNeil & Nelson (2009) the authors combine various techniques in the literature (Duncan et al. 1998; Chambers 1999; Saha & Tremaine 1992) to construct a new algorithm which allows for radial zones with different timesteps and different inter-zone force evaluation frequencies, but reduces to the proven techniques of Duncan et al. (1998) and Chambers (1999) for objects within the same zone. This allows new trade-offs between force accuracy and run time.

In our first paper, McNeil & Nelson (2009), we addressed the numerical challenges of studying oligarchic models of short-period exoplanet formation. Here we apply a new code with a parallel implementation of those methods, to determine the “reference population” of planets predicted by the fiducial models. We integrate global planetesimal discs extending from 0.05 AU to 10 AU under various models of the protoplanetary disc. Our models, both semianalytic and N-body, are described in §2, and the simulation conditions in §3. Simulation results are presented in §4 and discussed in §5, and we conclude in §6.

## 2 DESCRIPTION OF MODELS

To model the formation of planets in a global disc with a large dynamic range, we will divide the system into three stages: (1) the first stage, corresponding to the first 0.4 Myr after our nominal starting time  $t=0$ , which we will model using a semianalytic treatment based upon that of Thommes et al. (2003); (2) the middle stage, from  $t=0.4$  Myr to 6 Myr, which we will model using the new multiscale N-body code; and (3) the late post-gas stage, from 6 Myr to 100 Myr, during which we will evolve the inner regions of the disc using a traditional SyMBA implementation.

As usual, the semianalytic model serves two purposes. It allows for rough exploration of parameter space and provides self-consistent initial conditions for the second stage. In practice, we find that for the purposes of serving as initial conditions, the model is often more than is necessary: as long as the initial mass of the growing protoplanets is much less than their final mass, and they have many encounters before they undergo significant migration, the systems do not appear to show strong dependence on the details of the initial conditions. As a quasi-equilibrium, oligarchy is quite robust. Nevertheless, although using the model does not eliminate the problems caused by initial conditions with inconsistent histories, it does help mitigate them.

To explain our approach, we will first introduce the general features of the gaseous and solid material of the protoplanetary disc in sections 2.1 and 2.2, and then describe the prescriptions for the aerodynamic and type I drags applied to objects by the gas disc in sections 2.3 and 2.4. These

models are shared by both our semianalytic approach for the early stage, summarized in 2.5, and our N-body approach to the later stages, summarized in 2.6.

### 2.1 Gas disc

For simplicity we will consider only models resembling those of the minimum-mass solar nebula (MMSN) of Hayashi (1981), in which all physical disc parameters may be expressed as simple functions of the cylindrical radius from the star  $r$  and the height above the disc midplane  $z$ .

We take the volume density of the gas to be

$$\rho_{\text{gas}}(r, z) = \Sigma_{\text{gas}} / \sqrt{2\pi} z_0 \exp(-z^2/2z_0^2) \quad (1)$$

where  $(r, z)$  are cylindrical coordinates and  $z_0$  is the disc thickness. We set

$$\Sigma_{\text{gas}} = \Sigma_{1\text{AU}}^g (r/\text{AU})^{-\alpha} \quad (2)$$

where  $\Sigma_{1\text{AU}}^g$  is the gas surface density at 1 AU (1704 g/cm<sup>2</sup> in the MMSN) and  $\alpha$  gives the radial dependence of the density ( $\alpha = 1.5$  in the MMSN). In practice, the quantity of interest is usually the ratio of mass in the disc to the mass in the MMSN. We label this ratio  $f_{\text{enh}}$ , and determine the appropriate  $\Sigma_{1\text{AU}}^g$  by normalizing so that the amount of gas mass from 0.05 AU to 15 AU in each simulation is  $f_{\text{enh}}$  times the MMSN value. In general terms the disc masses that we adopt are consistent with disc masses inferred from submm observations (Andrews & Williams 2005, 2007). More specifically, Andrews & Williams (2005) indicate that more than one third of discs in the Taurus-Auriga region have masses which exceed that of the MMSN model, with similar statistics applying to discs observed in the  $\rho$  Ophiuchus complex (Andrews & Williams 2007).

For the disc height we take

$$z_0 = 0.0472 \text{ AU} (r/\text{AU})^{5/4} \quad (3)$$

Note that this power-law in  $r$  is traditional in the N-body planetary formation community but differs from the canonical choice in the planetary hydrodynamics community of taking a constant  $z_0/r$  ratio of 0.05 or 0.07. (Although the difference may appear minor, it changes the surface density power-law at which neighbouring equal-mass objects undergoing type I migration switch from convergent to divergent migration, and is known to be important when reconciling results from different simulations involving capture into resonance: see Cresswell & Nelson 2008.) We assume the gas is in perfect cylindrical rotation. We parametrize the pressure support by

$$\eta = 0.6(z_0/a)^2 \quad (4)$$

with typical  $\eta \simeq 0.001$ , and take

$$v_{\text{gas}} = v_{\text{kep}} \sqrt{1 - 2\eta} \quad (5)$$

where  $v_{\text{kep}}$  is the orbital velocity for a circular orbit at  $r$ .

The dissipation of the gas disc with time  $t$  is treated by introducing a single uniform exponential damping timescale,

$$\rho_{\text{gas}} \propto \exp(-t/\tau_{\text{decay}}) \quad (6)$$

following Kominami & Ida (2002). We neglect the gravitational potential due to the disc.

## 2.2 Solid material

At time  $t = 0$ , we set a fixed gas-to-rock ratio of  $\Sigma_{\text{gas}} = 240 \Sigma_{\text{rock}}$  (from the classical values of  $\sim 7 \text{ g/cm}^2$  for solids at 1 AU and  $\sim 1700 \text{ g/cm}^2$  for the gas, Hayashi 1981), and therefore take the initial surface density in rocky material to be of the form

$$\Sigma_{\text{rock}} = \Sigma_{1\text{AU}}^r (r/\text{AU})^{-\alpha} \quad (7)$$

where  $r$  is the cylindrical radius and  $\Sigma_{1\text{AU}}^r$  is the surface density of solids at 1 AU. After Thommes et al. (2003), we introduce a smoothed snow line beyond which the amount of material in solids is enhanced due to the temperature decreasing sufficiently to allow the condensation of ices. Placing the snow line at  $S_{1\text{oc}}$  and using a smoothing scale for the transition of  $S_{\text{sm}} = 0.25 \text{ AU}$ , and using an enhancement factor  $S_{\text{enh}}$ , we write

$$S = (0.5 \tanh((r - S_{1\text{oc}})/S_{\text{sm}}) + 0.5) \quad (8)$$

so that the total initial surface density in solids

$$\Sigma_{\text{solid}} = \Sigma_{\text{rock}}(1 - S) + S_{\text{enh}}\Sigma_{\text{rock}}(S) \quad (9)$$

The form of  $S$  is unimportant, and is chosen simply to soften the discontinuity for numerical purposes.

We assume that all solid material has a density of  $2.0 \text{ g/cm}^3$ .

## 2.3 Aerodynamic drag

We will apply an aerodynamic drag to all bodies (although the effects will usually be negligible on objects larger than 1000 km). We take the drag time-scale as

$$\tau_{\text{aero}} = \frac{8}{3} \frac{\rho_m}{\rho_{\text{gas}}} \frac{r_m}{C_D} \frac{1}{v_{\text{rel}}} \quad (10)$$

where  $\rho_m$  is the mass density of an object,  $r_m$  its radius,  $v_{\text{rel}}$  its velocity relative to the gas velocity at its position, and for simplicity we use a drag efficiency of  $C_D = 1$ . In our semianalytic model, we will use the approximately equivalent form

$$\tau_{\text{aero}} = \frac{1}{e_m} \frac{m}{(C_D/2) \pi r_m^2 \rho_{\text{gas}} a \Omega} \quad (11)$$

where  $m$  is the planetesimal's mass,  $a$  its semimajor axis,  $e_m$  its eccentricity, and  $\Omega$  its orbital frequency.

Orbit-averaging the above expression to determine the planetesimal migration rate  $v_m$  in the small  $e$ ,  $i$  (inclination), and  $\eta$  limit, Adachi et al. (1976) (after correction by Kary et al. 1993) find

$$v_m = \left. \frac{da}{dt} \right|_{\text{aero}} \simeq -2 \frac{a}{\tau_{\text{aero}} e_m} \left( \frac{5}{8} e_m^2 + \frac{1}{2} i_m^2 + \eta^2 \right)^{1/2} \left\{ \eta + \left( \frac{\alpha}{4} + \frac{5}{16} \right) e_m^2 + \frac{1}{8} i_m^2 \right\} \quad (12)$$

For the N-body code, we will use the acceleration

$$\mathbf{a}_{\text{aero}} = \frac{d\mathbf{v}}{dt} = \frac{\mathbf{v} - \mathbf{v}_{\text{gas}}}{\tau_{\text{aero}}} \quad (13)$$

with  $\tau_{\text{aero}}$  from eq. 10.

## 2.4 Type I migration

For semianalytic purposes, we use the type I migration equation of Tanaka et al. (2002), which gives an orbit-averaged migration rate  $dr/dt$  of

$$v_M = -c_a (2.7 + 1.1\alpha) \left( \frac{M}{M_\odot} \right) \left( \frac{\Sigma_{\text{gas}} r^2}{M_\odot} \right) \left( \frac{r}{z_0} \right)^2 r \Omega \quad (14)$$

for an object of mass  $M$  at distance  $r$  with orbital frequency  $\Omega$ , where we introduce  $c_a$  as a parameter to incorporate uncertainty in the migration efficiency. We note that significant contributions to the corotation torque may arise due to non-linear effects, resulting in a significantly reduced migration rate (Masset et al. 2006; Paardekooper & Papaloizou 2009), such that  $c_a < 1$ . The semianalytic model will assume that embryos are always on circular orbits and so we do not need an expression for the eccentricity damping.

For N-body calculations, we will use the full instantaneous specific force expressions of Tanaka et al. (2002) and Tanaka & Ward (2004), as given in appendix A of Daisaka et al. (2006), which we do not repeat here. Our only modification is to introduce a  $c_a$  parameter into the relevant radial migration term of the form of eq. 14.

There have been a number of developments over recent years which have led to modifications of the basic picture of how type I migration may operate under differing assumptions about the underlying protoplanetary disc structure. In addition to the corotation torque effects mentioned above, it has been noted that regions in the disc where the surface density profile has a positive gradient (such that the surface density increases outward) may act as planet traps, where planetary migration may not occur at all (Masset et al. 2006b). A planet trap may exist near to the star where the stellar magnetosphere clears a low density cavity in the disc (Lin et al. 1996). As discussed in the introduction to this paper, and in section 5.2, other researchers have considered the role of this cavity in the formation of short-period Neptune and super-Earth planets, and not surprisingly have found that the accumulation of planetary embryos there can lead to the formation of planets of the required mass. However, the formation of multiple Neptune and/or super-Earth-mass planet systems with a broad range of semimajor axes, such as HD69830, do not arise naturally from these models. Formation of a multiple planet system inside the cavity is possible, but the gravitational potential well of the star likely prevents scattering out to orbital radii that would be required to explain HD69830. Morbidelli et al. (2008) examined the possibility of planetary growth at a planet trap located near the snowline. Probably the most plausible explanation for a planet trap being located there is the model of inside-out disc clearance by magnetohydrodynamic turbulence suggested by Chiang & Murray-Clay (2007). The simulations by Morbidelli et al. (2008) indicate that multiple planets at a planet trap located at the snowline can indeed undergo close encounters and collisions through mutual scattering, allowing large bodies to grow there. In addition, scattering out of the trap was observed, allowing planets to migrate inward after growth through tidal interaction with the interior disc. One uncertainty which remains in this picture is how clear of material the inner disc needs to be for the inside-out clearing model of Chiang & Murray-Clay (2007) to operate. X-rays generated in the stellar corona need to be

able to penetrate deep into the disc and out to large radii for the planet trap to be located at the snowline, leading to uncertainty about how much type I migration can actually ensue once planets are scattered out of the trap. Given this uncertainty in the model, we have chosen to focus on the most generic type I migration scenario in the present study, which does not include planet traps located at specific radii.

## 2.5 Semianalytic approach

We follow McNeil et al. (2005), which is derived from Thommes et al. (2003), replacing only the formula for type I drag used there (due to Papaloizou & Larwood 2000) with that of Tanaka and Ward (eq. 14). We will forego repeating the derivations and simply describe the resulting equations.

We simulate the oligarchic migration formation scenario using a continuous two-component model consisting of protoplanetary embryos of mass  $M(a)$  which accrete mass from a planetesimal field distribution with surface density  $\Sigma_m(a)$  orbiting a star of mass  $M_\odot$ , with gravitational constant  $G$ . The embryos (of density  $\rho_M$ ) are assumed to be kept at a constant fixed separation  $b$  in single-planet Hill units ( $r_H = (M/3M_\odot)^{1/3}a$ ) as a consequence of the usual oligarchic equilibration between the increased separation due to scattering and the decreased separation due to accretion (Kokubo & Ida 1998). (As discussed in McNeil et al. 2005, this approximation is questionable at late times when strong migration is operating or the discs are very massive, but is reasonable during the early stages.) The embryo eccentricities are neglected as they are likely to be much smaller than those of the planetesimals due to both dynamical friction and type I damping (itself a kind of dynamical friction with the gas). The planetesimals (of density  $\rho_m$ ) are assumed to have a uniform mass  $m$  (and radius  $r_m$ ), and at a given semimajor axis all have an equilibrium eccentricity found by equating the time-scale for stirring by the embryos by damping by aerodynamic drag. See Chambers (2006) for a detailed description of the weaknesses of the equilibrium eccentricity assumption, and also note that by neglecting the contribution of embryo-embryo mergers we underestimate the accretion rate.

The physics in the model is simple, although the algebra is somewhat tedious. Embryos accrete mass from the planetesimals according to the expression<sup>2</sup>

$$\left. \frac{dM}{dt} \right|_{\text{accr}} = \frac{3.93 M_\odot^{1/6} G^{1/2} \Sigma_m M^{2/3} b^{2/5} C_D^{2/5} \rho_{\text{gas}}^{2/5}}{\rho_M^{1/3} a^{1/10} m^{2/15} \rho_m^{4/15}} \quad (15)$$

which corresponds to a decrease in planetesimal surface density

$$\left. \frac{d\Sigma_m}{dt} \right|_{\text{accr}} = \frac{-M_\odot^{1/3}}{3^{2/3} b \pi a^2 M^{1/3}} \frac{dM}{dt} \quad (16)$$

Planetesimals migrate due to aerodynamic drag with a radial rate  $v_m$  given by eq. 12, and embryos migrate due to type I effects with a radial rate  $v_M$  given by eq. 14. These four equations – 15, 16, 12, and 14 – are numerically integrated.

We will assume that the separation  $b = 10$  and that all planetesimals have  $r_m = 10$  km. We will take the initial seed mass for the embryos as  $M(a, t = 0) = 1.5 \times 10^{-3} M_\oplus$ , which has the effect of artificially accelerating the growth of the more distant embryos during the earliest stages.

## 2.6 N-body approach

The semianalytic Eulerian approach of the previous section can be useful as a rough estimate of the behaviour of the system, but contains very limited information about the dynamics involved. For later stages in which the interactions between the embryos are significant a particle-based Lagrangian approach using an N-body code is necessary.

Currently, the most robust N-body algorithm for oligarchic simulations of planet formation on long time-scales remains SyMBA (Duncan et al. 1998), which derives from the original mixed-variable symplectic integrators of Wisdom & Holman (1991) and Kinoshita et al. (1991) but has been improved to treat close encounters between particles. Unfortunately, it requires a common base timestep for all particles, which is set to some small fraction (typically  $\sim 1/15$  or less) of the innermost period so that pericentre passage is always resolved. (Levison & Duncan 2000 introduced a variant which could handle occasional objects crossing the usual innermost boundary by smoothly switching to a Bulirsch-Stoer integrator, following up on the innovations of Chambers 1999, but it becomes impractical when boundary crossings are common.) In a companion paper (McNeil & Nelson 2009) we introduce a new algorithm NAOKO which allows for multiple radial zones with distinct timesteps and can vary the number of force evaluations between different zones, making possible a new trade-off between the force accuracy between distant objects and speed. We have implemented a parallel version of NAOKO in the planet formation code MIRANDA, which is basically a parallel SyMBA implementation.

As in the semianalytics, we have two classes of objects, embryos and planetesimals, where the embryos can merge with each other and with the planetesimals, but the planetesimals do not self-interact either gravitationally or collisionally. Two objects (assumed spherical) merge if their physical separation is less than the sum of their physical radii, and form one new object, conserving mass and linear momentum. No fragmentation is considered. Following standard practice (e.g. Thommes et al. 2003) we use “super-planetesimals”, and replace the planetesimals of mass  $m$  we would prefer to use with larger objects of mass  $m_{\text{sp}}$  which behave as objects of mass  $m$  with respect to non-gravitational interactions like gas drag, and serve as representative elements of an underlying planetesimal population. As long as the number of super-planetesimals is large and the embryo mass is greater than the super-planetesimal mass ( $M \gg m_{\text{sp}}$ ), the accretion rate is insensitive to this approximation. (Taking a uniform  $m$  for the planetesimals and neglecting their self-interactions are considerably more damaging simplifications than using super-planetesimals in any event.)

Interactions with the gas disc are limited to aerodynamic drag and type I drag, as described in sections 2.3 and 2.4. The super-planetesimals will experience an aerodynamic drag corresponding not to the physical radius of the

<sup>2</sup> The factor of  $b^{2/5}$  is missing from eq. 4 of McNeil et al. (2005); the error was typographical.

integrated tracer, but to that of the underlying planetesimal (typically  $\simeq 10$  km).

For the computationally challenging second stage during which the gas is present, we will integrate the system using MIRANDA in its new NAOKO mode (McNeil & Nelson 2009). This allows the disc to be divided into distinct radial zones, and objects in each zone are integrated using different time steps. In the simulations presented here we used four zones, with timesteps chosen so that all objects had at least  $\simeq 15$  steps per orbit: namely,  $\Delta t = 0.53$  yr for objects outside 4 AU;  $\Delta t = 0.13$  yr for 1.6–4 AU;  $\Delta t = 0.013$  yr for 0.34–1.6 AU; and  $\Delta t = 0.00083$  yr for 0.05–0.34 AU. This corresponded to timestep ratios between outer and inner zones of 4, 10, and 16, respectively. These ratios also describe the ratios of the frequencies on which the interzone forces were evaluated; intrazone forces were evaluated at each (zone) step. Boundaries between zones had associated transition zones centred there, of widths 0.5 AU, 0.1 AU, and 0.04 AU from outermost to innermost, in which the objects smoothly experienced both timesteps to avoid artificial kicks in velocity. For the late stage after the gas disc has dissipated, the number of particles in the inner zone of interest will have decreased enough that we can return to the traditional SyMBA method to simulate the final giant-impact stage, with a fixed timestep of 0.0007 yr.

### 3 SIMULATION CONDITIONS

Computational power being limited, it was not feasible even with the new code to perform multiple runs for each parameter set of interest. Instead, we made compromises between coverage of parameter space and reproducibility of each run, and between concentrating on physically plausible scenarios and less plausible but informative limiting cases. Table 1 lists the resulting choices, and where two simulation labels are given we ran two instantiations which differed only in the random number seeds used to define the initial Keplerian angular variables of the particles.

We used mass enhancement factors of  $f_{\text{enh}} = 3, 5, 10$ , to cover the range from the likely enhancements above the MMSN needed to form the solar system to something considerably larger. (Again,  $\Sigma_{1\text{AU}}^g$  is determined from normalizing the amount of mass between 0.05 AU and 15.0 AU to be  $f_{\text{enh}}$  times the MMSN value.) The surface density power-law was chosen from  $\alpha = 1.0, 0.5, 0.001$ , so that the discs are all much flatter than the MMSN (with  $\alpha = 1.5$ ). The MMSN value was skipped in the production runs presented here because preliminary low resolution simulations indicated that disc models with a high degree of central mass concentration do not successfully form surviving short-period planetary systems with significant amounts of mass. This may be due in part to the fact that such a disc model induces divergent type I migration for neighbouring bodies of equal mass, as discussed below, thereby reducing the planetary growth rate. In addition, viscous disc models based on the Shakura & Sunyaev (1973) ‘alpha’ prescription for viscosity tend to generate shallower surface density distributions (Papaloizou & Terquem 1999; Fogg & Nelson 2007). Note that with  $z_0/r \propto r^{1/4}$  (eq. 3), the type I  $dr/dt$  rate is independent of  $a$  for equal M at  $\alpha = 1.0$ , and shows convergent migration for  $\alpha < 1.0$ . We used disc dissipation time-scales

**Table 1.** Simulation parameters.

Simulation	$f_{\text{enh}}$	$S_{\text{loc}}$ [AU]	$\alpha$	$c_a$	$\tau_{\text{decay}}$ [Myr]
S01A, S01B	3	2.7	0.001	0.3	1
S02A	3	2.7	0.001	0.3	2
S03A, S03B	3	2.7	0.001	1.0	1
S04A	3	2.7	0.001	1.0	2
S05A, S05B	3	2.7	0.5	0.3	1
S06A	3	2.7	0.5	0.3	2
S07A, S07B	3	2.7	0.5	1.0	1
S08A	3	2.7	0.5	1.0	2
S09A, S09B	3	2.7	1.0	0.3	1
S10A, S10B	3	2.7	1.0	1.0	1
S11A	3	2.7	1.0	1.0	2
S12A, S12B	5	2.7	0.001	0.3	1
S13A	5	2.7	0.001	0.3	2
S14A, S14B	5	2.7	0.001	1.0	1
S15A	5	2.7	0.001	1.0	2
S16A, S16B	5	2.7	0.5	0.3	1
S17A, S17B	5	2.7	0.5	1.0	1
S18A	5	2.7	0.5	1.0	2
S19A, S19B	5	2.7	1.0	1.0	1
S20A	10	2.7	0.5	0.3	1
S21A	10	2.7	0.5	1.0	1
S22A	10	2.7	1.0	0.3	1
S23A	3	4	0.001	0.3	1
S24A	3	4	0.001	1.0	1
S25A	3	4	0.5	0.3	1
S26A	3	4	0.5	1.0	1
S27A	3	4	1.0	0.3	1
S28A	3	4	1.0	1.0	1
S29A	5	4	0.001	0.3	1
S30A	5	4	0.001	1.0	1
S31A	5	4	0.5	0.3	1
S32A	5	4	0.5	1.0	1
S33A	5	4	1.0	0.3	1
S34A	5	4	1.0	1.0	1
S35A	10	4	0.5	1.0	1
S36A	10	4	1.0	0.3	1
S37A	10	4	1.0	1.0	1

(eq. 6) of 1 Myr and 2 Myr, which are roughly compatible with the observed disc decay times inferred from observations (e.g. Haisch et al. 2001). The migration efficiency  $c_a$  was set to either 0.3 or 1.0. The snow line was placed at either  $S_{\text{loc}} = 2.7$  AU or 4.0 AU, with an enhancement factor of  $S_{\text{enh}} = 4$ . Some studies suggest that a snow line closer to the star (1.6–1.8 AU, Lecar et al. 2006) and a lower enhancement factor ( $\sim 2.2$ , Lodders 2003) may be more realistic, but others argue that a much higher enhancement can occur (Ciesla & Cuzzi 2006). Since many of the Neptune-mass objects found to date orbit lower-luminosity stars, a closer-in snow line may more accurately model the environments of the known short-period Neptune planets. However, to facilitate comparison with other work we will keep the mass of the central star at  $M_{\odot}$  and use the historical snow line. (The  $S_{\text{loc}} = 4.0$  AU runs were an experiment motivated by some preliminary simulations which suggested that delaying the onset of embryo growth past the snow line could help prevent promising objects from falling into the star; c.f. Chambers 2006.)

Each simulation was evolved for the first 0.4 Myr using the semianalytic model of §2.5. This yielded a distribution of embryo mass  $M(a)$  and planetesimal surface density  $\Sigma_m(a)$ . These were then discretized into an N-body particle distribu-

tion extending from 1 AU to  $\sim 10$  AU, with spacing between the embryos fixed at  $b \simeq 10$  and the super-planetesimal mass  $m_{\text{sp}}$  chosen to ensure that locally  $M/m_{\text{sp}} \geq 5$  with  $r_m = 10$  km. (This is a somewhat more relaxed condition than used in McNeil et al. (2005), which required the relationship to hold globally and used one uniform  $m_{\text{sp}}$ .) The resulting particle sets had between 40 and 64 fully interacting embryos, with  $> 10000$  super-planetesimals for the main  $S_{\text{loc}} = 2.7$  AU runs and  $\sim 4000$  super-planetesimals for the lower-resolution  $S_{\text{loc}} = 4.0$  AU experiments. The initial embryo eccentricities and inclinations were arbitrarily set to 0.001 and 0.0005, respectively, and the planetesimal eccentricities to their (semianalytically-estimated) equilibrium values. The simulations rapidly reach their random-velocity equilibrium. The particle distributions were then integrated until  $t=6$  Myr using the NAOKO algorithm of §2.6. This 6 Myr time-scale was chosen so that even in the simulations with  $\tau_{\text{decay}} = 2$  Myr, at least 95% of the original gas mass is gone. Finally, the resulting protoplanets inside of 2 AU were then integrated until  $t=100$  Myr using the traditional SyMBA algorithm. (That is, the remnant planetesimal disc was removed entirely, as were all embryos with semimajor axis  $> 2$  AU.)

Each integration took roughly 3  $\sim$  4 weeks of runtime on an 8-processor node for the 0.4-6 Myr phase, and then another week to two weeks in serial mode for the 6-100 Myr phase. Without the use of both parallelism and the new NAOKO algorithm, the simulations would have taken an impractically long time.

## 4 RESULTS

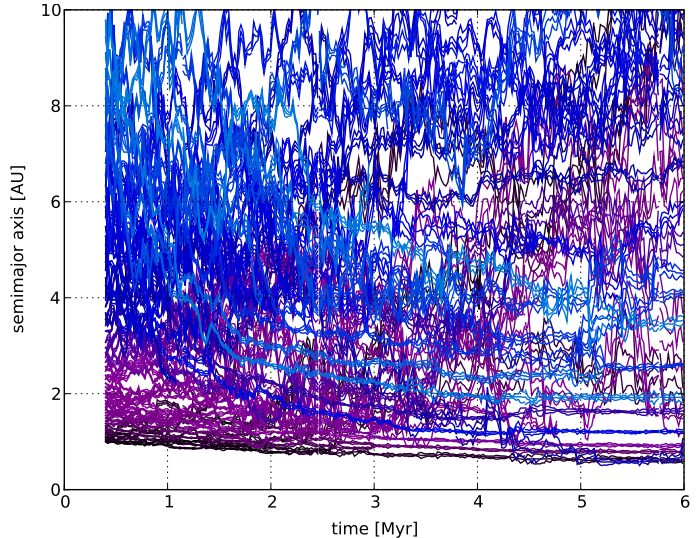
In this section we present some sample runs in §4.1, including both representative cases showing the radial evolution of the embryos in §4.1.1 and the evolution of a few of our “successful” runs in §4.1.2 and §4.1.3. We discuss the global results in §4.2, giving an overview in §4.2.1. The planetary mass distributions are covered in §4.2.2; the distribution of ices in §4.2.3; various statistics on the resulting configurations in §4.3; the final number of planets and the radial mixing in §4.3.1; the total surviving mass in the inner region in §4.3.2; and, finally, the possibility of future mergers and the long-term stability of the systems in §4.3.3.

### 4.1 Description of individual runs

#### 4.1.1 Sample migration histories

Figures 1, 2, and 3 offer example overviews of the radial evolution of the embryos. In S14A, a flat disc ( $\alpha = 0.001$ ) with moderate enhancement  $f_{\text{enh}} = 5$ , the outer regions are still chaotic at 6 Myr. In S07A, a steeper disc with  $\alpha = 0.5$  and low enhancement  $f_{\text{enh}} = 3$ , an object from beyond the snow line grows massive enough sufficiently early to migrate inwards much faster than its neighbours and compress the earlier objects into a much smaller radial region, causing both mergers and occasional outward ejections (e.g. just after 2 Myr). There is little communication between the innermost and the outermost regions, creating a large empty region in  $(a, t)$  space devoid of planetary embryos. In S19A,  $\alpha = 1.0$  with moderate enhancement  $f_{\text{enh}} = 5$ , we see that almost all

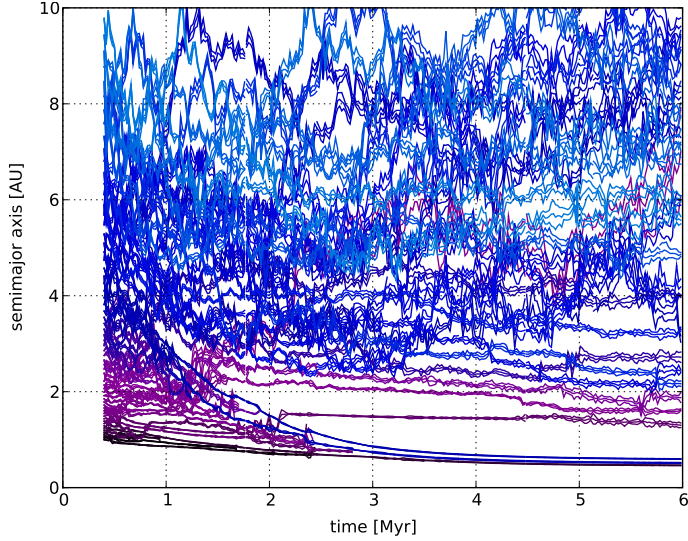
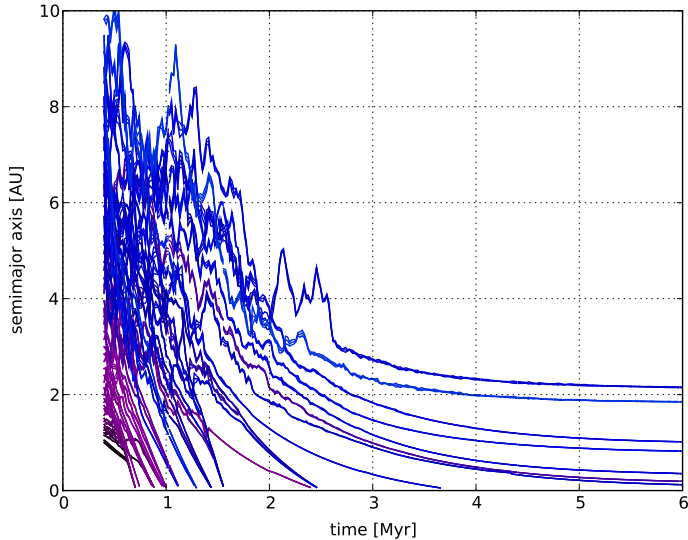
**Figure 1.** Semimajor axis, perihelion, and aphelion for each embryo over time in simulation S14A.



of the inner material is rapidly lost to the inner edge of the simulation, and much of the material which eventually forms the resulting inner system comes from far beyond the snow line. However, some of the resulting planets incorporate material which started inside of the snow line and was scattered out beyond it before migrating back in. Each simulation had  $c_a = 1.0$  and  $\tau_{\text{decay}} = 1$  Myr, and therefore the majority of their tidal migration is complete by 3 Myr, although as S14A shows, a considerable amount of radial migration can continue due to embryo-embryo interactions long after the gas disc is gone. This can be compared with McNeil et al. (2005)’s study of terrestrial planet oligarchic migration scenarios, which predicted a tripartite division into an interior region of strong convoying behavior (where planets rapidly lock into mean-motion resonance and migrate in tandem), a transition region where objects ‘slide’ towards their final destinations, and an outer region which remains chaotic. In their study, they looked only at the  $\alpha = 1.5$  and  $\alpha = 1.0$  cases, and did not consider any  $\alpha$  generating convergent migration.

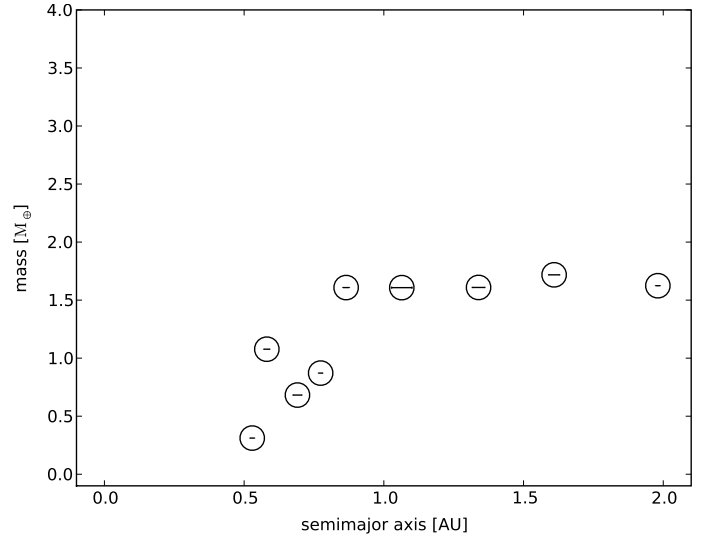
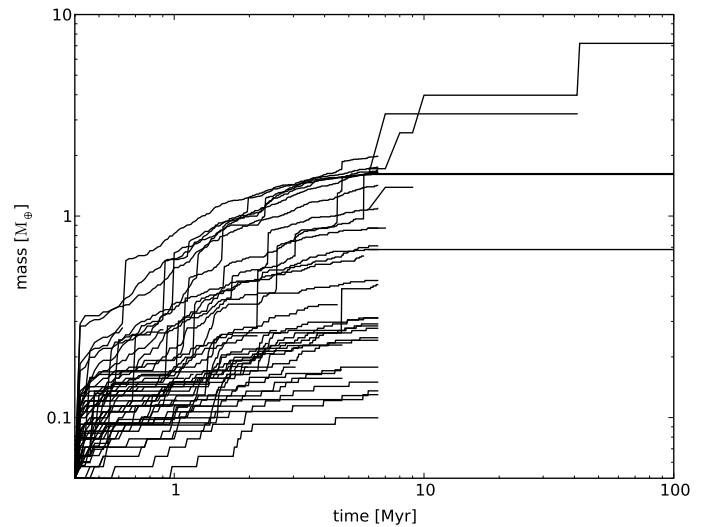
#### 4.1.2 Run S09A

The run S09A produced the single most massive object of any simulation, a planet of  $7.2 M_{\oplus}$ . This particular run had the parameters  $f_{\text{enh}} = 3$ ,  $\alpha = 1.0$ ,  $c_a = 0.3$ ,  $\tau_{\text{decay}} = 1$  Myr, and  $S_{\text{loc}} = 2.7$  AU. At  $t=0.4$  Myr, the simulation start, there were roughly comparable amounts of mass in embryos and planetesimals inside of 2 AU,  $M_{\text{tot}}=1.1 M_{\oplus}$  and  $m_{\text{tot}}=1.4 M_{\oplus}$ , respectively. By 1 Myr, both have increased, to  $M_{\text{tot}}=2.3 M_{\oplus}$  and  $m_{\text{tot}}=1.8 M_{\oplus}$ . The amount of embryo material in the region gradually increases to  $11.1 M_{\oplus}$  at 6 Myr. This increase is non-monotonic, as embryos are occasionally lost in two ways. First, some are scattered beyond the inner simulation edge at 0.05 AU where they are removed. Second, some are scattered beyond the 0.05-2 AU window, in which case they will remain in the system but no longer contribute to the mass (at least unless type I migration or embryo-embryo scattering brings them back

**Figure 2.** Semimajor axis, perihelion, and aphelion for each embryo over time in simulation S07A.**Figure 3.** Semimajor axis, perihelion, and aphelion for each embryo over time in simulation S19A.

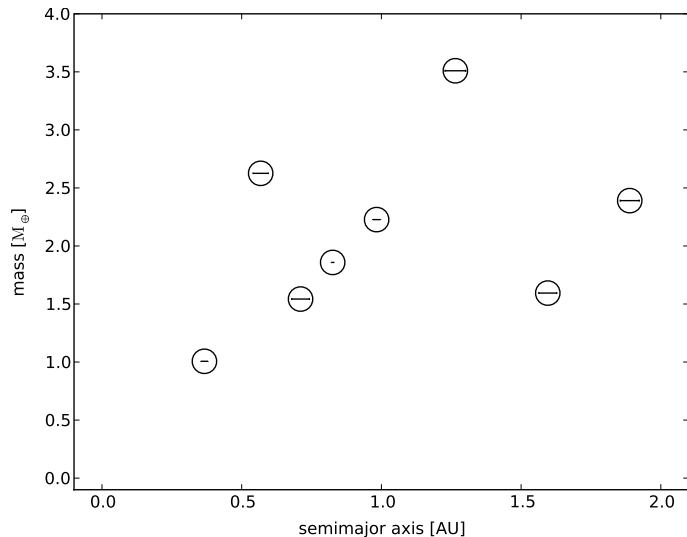
in again). By contrast, the planetesimal material reaches a maximum of  $\simeq 2.3M_{\oplus}$  at 2.2 Myr, as it migrates into the region via both Jacobi shepherding by embryos and aerodynamic drag, and then falls off to  $\simeq 1.5M_{\oplus}$  for the remainder of the simulation, as material is consumed but new material is brought in to replace it.

As shown in figure 4, at 6 Myr there are nine embryos with  $a < 2$  AU, and they fall into two distinct categories: four objects inside of 0.8 AU, with masses less than  $1.2 M_{\oplus}$  which vary by factors of three, and five well-spaced objects exterior to 0.8 AU which all have masses  $\simeq 1.6 - 1.7M_{\oplus}$ , where the inner three have startlingly similar masses, namely  $1.608 M_{\oplus}$ ,  $1.609 M_{\oplus}$ , and  $1.607 M_{\oplus}$ . Figure 5 shows that this is simply a coincidental result of equilibration processes, as the objects follow roughly similar growth curves – an early period of fast accretion transitioning to a much slower phase after 3 Myr when the gas is

**Figure 4.** Run S09A planets interior to 2 AU at  $t=6$  Myr, planet mass versus semimajor axis, with bars indicating eccentric excursion.**Figure 5.** Run S09A planet mass versus time for all objects. From  $t=6$  Myr, only the embryos interior to 2 AU are followed.

mostly gone – but at times the objects differ in mass by a factor of  $\simeq 2$ . The three  $\sim 1.61M_{\oplus}$  objects also come from very different locations in the disc: the outermost embryo started its life at 2.4 AU, the middle at 3.3 AU, and the innermost at 1.6 AU. During the giant impact phase, the objects at 0.87 and 1.06 AU merge quite quickly, at  $\sim 7$  Myr, as do the two innermost bodies. By  $\sim 40$  Myr, the original ( $t=6$  Myr)  $1.7 M_{\oplus}$  body has consumed three more objects to reach its terminal mass, while the remaining objects were scattered outside 2 AU.



**Figure 6.** Run S16B planets at  $t=6$  Myr.


#### 4.1.3 Run S16B

The run S16B produced the largest amount of surviving embryo mass interior to 2 AU at 100 Myr of all the simulations,  $16.75 M_{\oplus}$ . This particular run had the parameters  $f_{\text{enh}} = 5$ ,  $\alpha = 0.5$ ,  $c_a = 0.3$ ,  $\tau_{\text{decay}} = 1$  Myr, and  $S_{\text{loc}} = 2.7$  AU. This region started with  $M_{\text{tot}}=1.00 M_{\oplus}$  and  $m_{\text{tot}}=1.3 M_{\oplus}$ , reaching final values of  $M_{\text{tot}}=16.8 M_{\oplus}$  and  $m_{\text{tot}}=1.9 M_{\oplus}$  at 6 Myr.

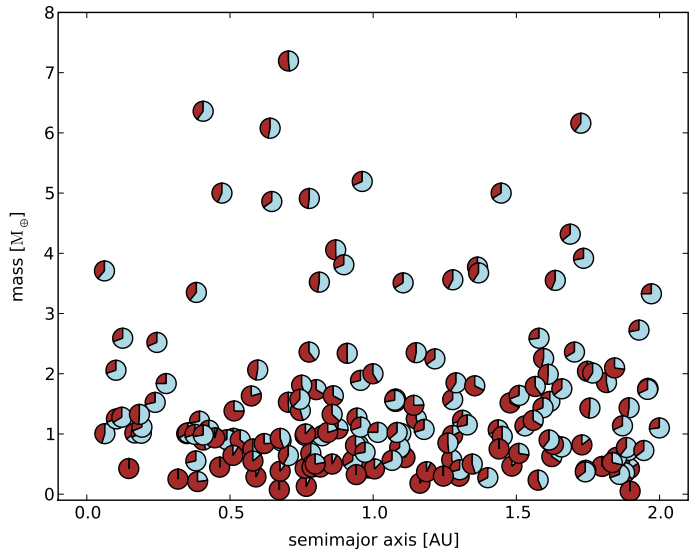
As shown in figure 6, there are 8 embryos with at least an Earth mass of material (including a hot Earth of  $1.01 M_{\oplus}$  at 0.37 AU). The planet masses vary more than in S09A, although it is still true that the planets with the lowest masses are on the interior and the highest masses have semimajor axes between 1.2 and 1.6 AU. The system is basically quiescent until a burst of activity between 14 and 15 Myr, during which the planet at 1 AU merges with the planets at 0.7 AU and 1.9 AU, and the planet at 0.6 AU merges with the planets at 0.8 AU and 1.6 AU. After this, the system does nothing but exchange angular momentum with little variation in semimajor axis.

Comparing S09A with S16B suggests that maximizing the mass of the final planet does not require maximizing the mass of the planets when the giant impact phase begins; both simulations produced maximum objects of mass 6 –  $7M_{\oplus}$ , despite S16B having 1.5 times the mass of S09A at 6 Myr.

## 4.2 Synthesis of simulation outcomes

### 4.2.1 Overview

Snapshots of the planetary systems which resulted at  $T=100$  Myr are shown in figures 7 and 8, with each planet being represented by a pie showing its fraction of rock and ice, and with horizontal bars indicating the eccentric excursion (and not, as is often done,  $\pm 5$  Hill radii.) It is worth noting that the maximum ice fraction possible is 0.75. Bodies composed entirely of material whose provenance lay interior to the snow line are 100% rock. Several general features of

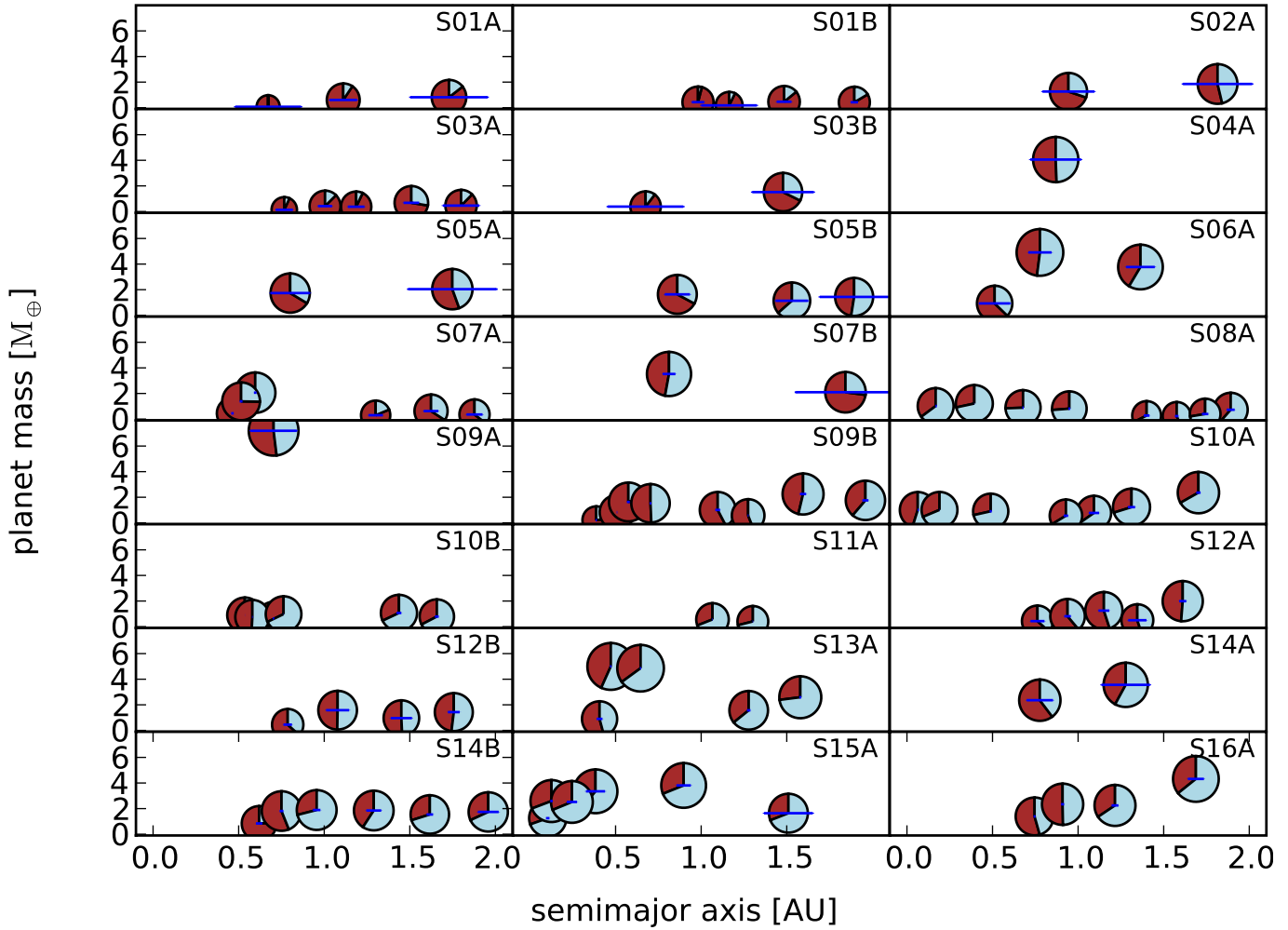
**Figure 9.** Set of final planets at  $t = 100$  Myr, planet mass versus semimajor axis. Pies as in fig. 7.


the simulation outcomes are immediately apparent in these figures.

Most of the objects, especially the smallest ones, have modest eccentricity. S07B and S17B are exceptions, in which the outermost body has a nonnegligible  $e$  (0.16 and 0.29, respectively.) There is also the case of S24A, which is manifestly unstable. The two outer planets had been exchanging  $a$  and  $e$  since an order-swapping encounter at 70 Myr, and had suffered a series of particularly close encounters  $\simeq 5$  Myr before the end of the simulation. It might have been expected that all of the larger objects would have the smallest eccentricities due to dynamical friction and type I drag, but once the gas disc has dissipated and the local planetesimals have been consumed, the remaining large planets can generate significant eccentricities.

It is also clear that stochasticity is playing a very important role. While in some cases the same initial conditions generate similar final configurations even after the variation of the angles (e.g. S01A/B, S05A/B), in other cases the resulting systems have almost no resemblance to each other (e.g. S09A/B, S14A/B, S17A/B). This confirms the regrettable fact that the simulation outcomes are sufficiently sensitive to the details of the encounter and merger history that isolated runs convey limited information, although they can certainly demonstrate that a given scenario is possible.

Figure 9 shows the complete collection of resulting planets (combined from all simulations). The majority of objects we form are small: the median planet mass is  $1.07 M_{\oplus}$ , and 90% of the objects have masses below  $3.55 M_{\oplus}$ . Defining success as the production of an object with greater than  $4 M_{\oplus}$  interior to 2 AU, there were only eight successful runs: S04A, S06A, S09A, S13A (2 objects), S16A, S16B (2), S17B (2), and S33A. Only one object (in S33A) came from a run with  $S_{\text{loc}} = 4$  AU, and so our early, mildly encouraging experiments with a more distant snow line proved unfruitful in the production runs. 5 of the 7 successes (not double-counting S16) had  $f_{\text{enh}} = 5$ , 2 had  $f_{\text{enh}} = 3$ , and – significantly – none had  $f_{\text{enh}} = 10$ . 5 of the 7 successes had



**Figure 7.** Final planetary systems at  $t = 100$  Myr by simulation, planet mass in Earth masses versus semimajor axis in AU. Each planet is plotted as a pie with radius proportional to its physical radius, with the blue (brown) slice corresponding to the fraction of its mass in ice (rock). Horizontal bars describe the eccentric excursion, i.e. they extend from  $a(1 - e)$  to  $a(1 + e)$ . The labels specify the simulation reference number as listed in table 1.

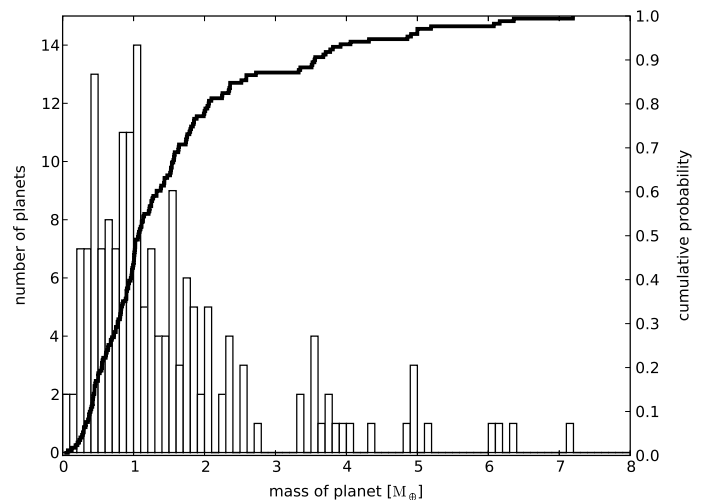
$c_a = 0.3$ . Every  $\alpha$  value generated at least one success (2, 3, 2 for  $\alpha = 0.001, 0.5, 1.0$ , respectively), and likewise for  $\tau_{\text{decay}}$  (4 for 1 Myr, 3 for 2 Myr). The single most successful parameter set was that associated with S16A and S16B, namely  $f_{\text{enh}} = 5, \alpha = 0.5, c_a = 0.3, \tau_{\text{decay}} = 1$  Myr,  $S_{\text{loc}} = 2.7$  AU.

It bears noting that the combined plots and histograms that we present in this section should be interpreted as ‘population synthesis’ only in a loose sense. There have been no corrections made for the shape of the parameter space, which includes duplications of some parameter runs, and which was not chosen to match any expected distribution of disc parameters in actual protoplanetary systems. Accordingly, they should be taken merely as summaries of our particular outcomes, and not as predictions for what any real-world observer would see.

#### 4.2.2 Planetary mass distribution

Keeping that warning in mind, figure 10 shows the number of bodies of a given mass produced across all the simulations.

**Figure 10.** Summary of planet mass outcomes.



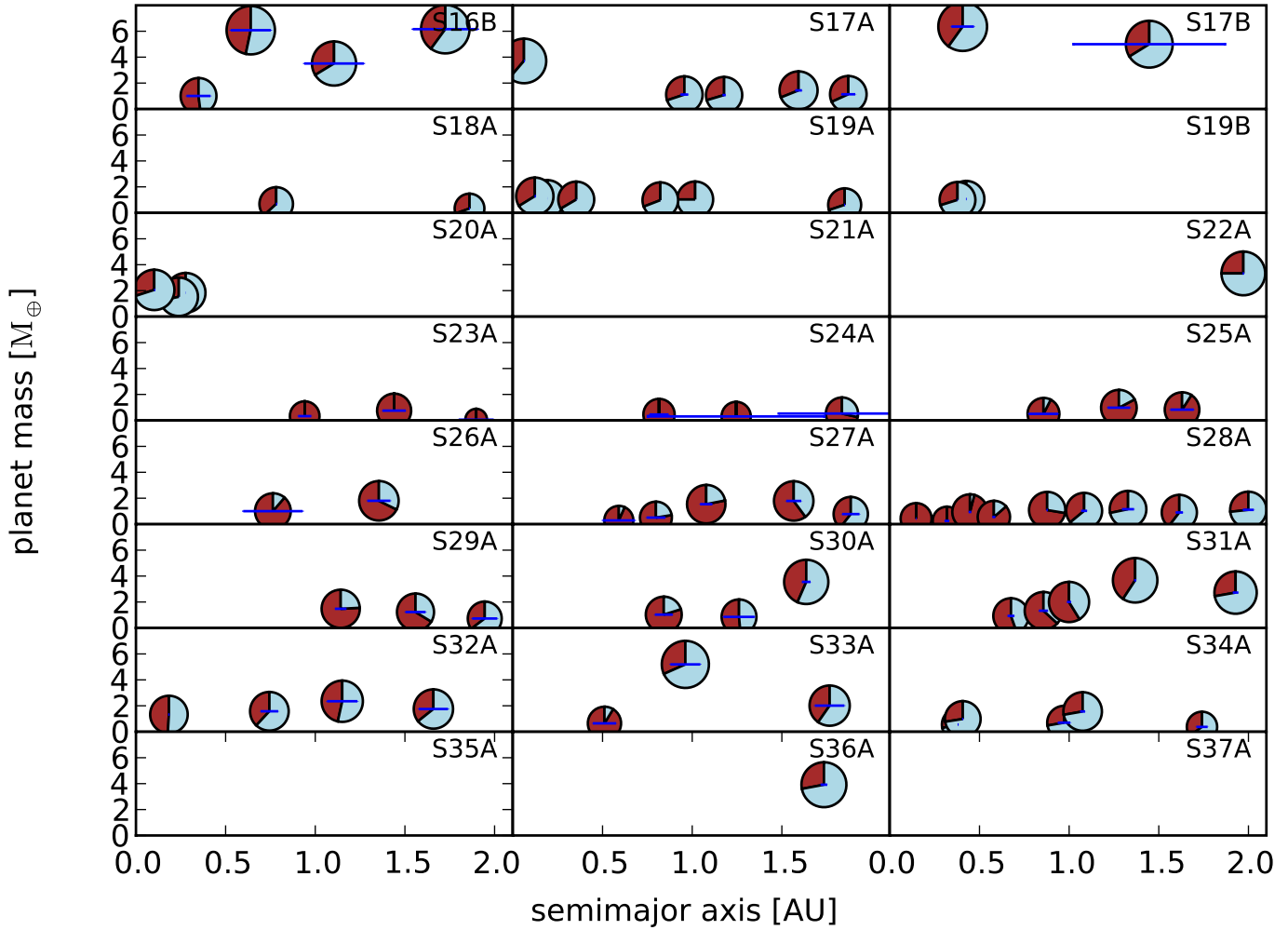


Figure 8. Final planets at  $t = 100$  Myr; as in fig. 7.

As mentioned previously, half of the planets formed have mass  $\leq 1M_{\oplus}$ . Beyond  $3M_{\oplus}$ , the numbers fall off dramatically. This is in agreement with some (unpublished) early exploratory low-resolution runs which had great difficulty forming planets greater than  $4M_{\oplus}$  regardless of the disc enhancement used. The median mass reached in the simulations is a full order of magnitude – 17 times – smaller than Neptune.

We can also consider not only the successful runs (in which we have small-number statistics problems) but look at the complete dataset: see table 2. Perhaps unsurprisingly, the greater the enhancement factor, the greater the median mass. However, this increase in the median value does not correspond to an increase in the maximum; indeed, the greater the enhancement  $f_{\text{enh}}$ , the *smaller* the resulting maximum mass of a planet. A more robust measure is the change in the mean mass of the top quintile, which shows that  $f_{\text{enh}} = 5$  produced more large bodies than  $f_{\text{enh}} = 10$ . A similar wrap-around occurs with  $\alpha$ , where  $\alpha = 0.5$  has a higher median and top-quintile-mean than either  $\alpha = 0.001$  or  $\alpha = 1.0$ . The existence of such maxima in parameter space suggests that some natural methods for increasing the planet growth rate – such as simply increasing the initial surface density of the disc – may not help increase the final

mass, as there are feedback mechanisms operating which resist the formation of larger bodies (namely the rapid inward migration of massive bodies which form early in a gas-rich environment). In part, this result could merely be statistical noise, as of the 7 simulations with  $f_{\text{enh}} = 10$ , only 3 produced planets (and all of those had weak migration with  $c_a = 0.3$ ), but this low number is itself an example of the problem. This agrees with the predictions of Daisaka et al. (2006), and (except at very high disc masses) with the results of Chambers (2008).

Table 2 reveals several other (apparent) correlations between the simulation parameters and the resulting planet masses beyond those involving  $f_{\text{enh}}$  and  $\alpha$ . Decreasing the migration efficiency ( $c_a$ ) improved the final mass, changing the median mass from  $1.0M_{\oplus}$  to  $1.4M_{\oplus}$  and the top quintile mean from  $3.0M_{\oplus}$  to  $4.5M_{\oplus}$ . The use of a more distant  $S_{\text{loc}} = 4$ , contrary to some of our early experiments, tended to reduce the planet mass. Finally, the runs with  $\tau_{\text{decay}} = 2$  Myr had smaller masses than those with  $\tau_{\text{decay}} = 1$  Myr, suggesting that the ability to bring in mass from farther out in the disc can overcome the loss of material to the star (or, at least, the simulation edge.) However, given the wide variation in outcomes for the same parameter set – and our use of no more than two instantiations of each – these results

**Table 2.** Summary of resulting planets by parameter; values are taken over all planets produced in the subset of runs with parameter = value.

Parameter	Value	planetary mass statistics [ $M_{\oplus}$ ]		
		Median	Maximum	Mean of top quintile
$f_{\text{enh}}$	3	0.826	7.194	2.667
$f_{\text{enh}}$	5	1.455	6.359	4.428
$f_{\text{enh}}$	10	2.058	3.917	3.917
$\alpha$	0.001	1.025	5.000	3.353
$\alpha$	0.5	1.412	6.359	4.478
$\alpha$	1.0	0.987	7.194	2.878
$S_{\text{loc}}$	2.7 AU	1.124	7.194	3.980
$S_{\text{loc}}$	4.0 AU	0.982	5.193	2.901
$c_a$	0.3	1.430	7.194	4.482
$c_a$	1.0	1.014	6.359	3.030
$\tau_{\text{decay}}$	1 Myr	1.044	7.194	3.447
$\tau_{\text{decay}}$	2 Myr	1.250	5.000	4.402

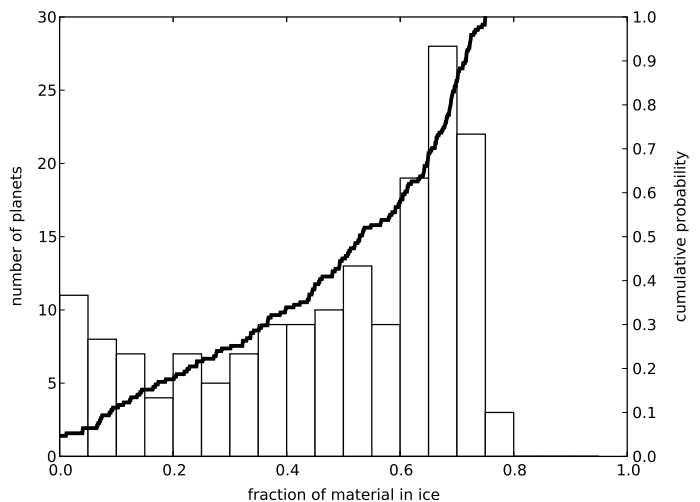
should be treated cautiously, despite our averaging over the suite.

In some runs, a considerable amount of mass was removed from the simulation by falling off our inner boundary of 0.05 AU. In the  $f_{\text{enh}}=10$ ,  $S_{\text{loc}}=2.7$  AU runs S20A, S21A, and S22A, the lost planets totalled  $34 M_{\oplus}$  (with the maximum mass of a lost planet being  $5.2 M_{\oplus}$ ),  $38 M_{\oplus}$  (maximum  $4.0 M_{\oplus}$ ), and  $67 M_{\oplus}$  (maximum  $7.1 M_{\oplus}$ ). (The continuous, fixed-spacing semianalytics generating the initial conditions are probably unreliable at such a large enhancement.) In the  $f_{\text{enh}} = 3$  and  $f_{\text{enh}} = 5$  cases, the amount of mass lost varied from none (in all the discs with  $\alpha = 0.001$  except S15A, which had  $c_a = 1$  and  $\tau_{\text{decay}} = 2$  Myr) to  $21\text{--}24 M_{\oplus}$  in S18A and S19A/B. Excluding the  $f_{\text{enh}}=10$  cases, none of the lost bodies were larger than  $3.3 M_{\oplus}$  (in S16A), and the median mass of a body which was lost was  $1.9 M_{\oplus}$ .

#### 4.2.3 Ice fractions

Figure 9 demonstrates that larger-mass objects tend to have higher ice fractions, and given our initial assumption that 75% of the material past the snow line was in ices, the ice fraction is a proxy for the radial transport. The median ice fraction for objects greater than  $1 M_{\oplus}$  is 0.60, and for objects smaller, 0.36. There were only 7 objects which contained no ices at all (1 from S01A; 3 from S23A; 2 from S24A; 2 from S28A), and all but one of those had masses smaller than  $0.5 M_{\oplus}$ , the exception having  $0.75 M_{\oplus}$ . Every ice-free body was formed from a run with  $f_{\text{enh}} = 3$  and  $\tau_{\text{decay}} = 1$  Myr, suggesting that we should only expect to find completely rocky bodies in low-enhancement discs with short disc lifetimes. Moreover, all but one ice-free planet was from a simulation with  $S_{\text{loc}} = 4$  AU, which suggests that in the more physically realistic scenarios we should expect almost no bodies which fail to contain material from beyond the snow line. (Of course, ‘ice-free’ and ‘completely rocky’ here are relative to the assignment of ice fractions at  $t=0.4$  Myr, when our N-body integrations began, although they should be assigned in a way consistent with the snow enhancement.) It is notable, as shown in figure 11, that the entire range of possible ice fractions is covered, from bodies which are completely ice-free to bodies which reach the maximal 75% value.

Figure 12 shows that the lower the ice fraction, the more

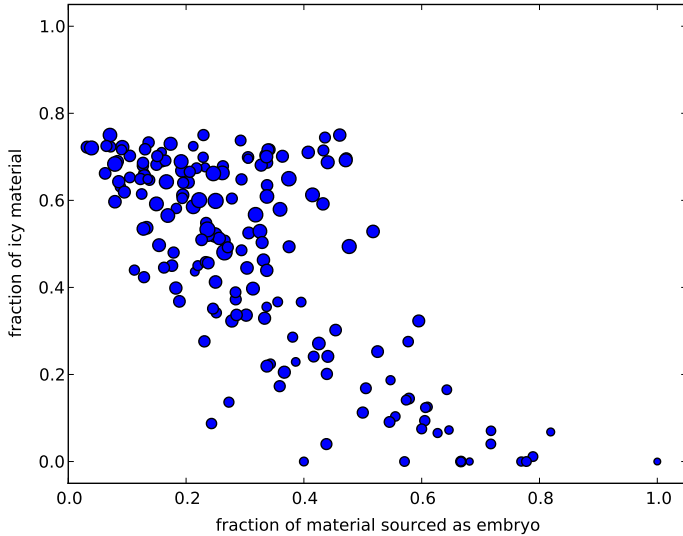
**Figure 11.** Summary of ice fraction outcomes.

of an object’s mass was consumed (or started) as an embryo, and not a planetesimal. At the start of the simulation, all embryos are either inside the snow line, in which case we assume they are composed entirely of rock, or outside the snow line, in which case we assume they are composed of 75% ice and 25% rock. (We neglect the early semianalytic evolution of the models before  $t = 0.4$  Myr; as a result, we slightly underestimate both the initial ice fractions of embryos in the inner regions and their consumption of planetesimals.) Accordingly, at  $t=0.4$  Myr, all embryos are either located at (1, 0) or (1, 0.75) on this plot: they are composed entirely of embryo material, and have ice fractions of either 0 or 0.75.

At first, objects located in both regions accrete local material from both embryos and planetesimals, which decreases their embryo fractions, but leaves their ice fractions constant as they accrete from nearby material which has the same ice fractions as they do (whether 0 or 0.75). Both interior and exterior objects therefore move left on the diagram. Eventually migration becomes important, which tends to move ice-rich material into the inner regions. Accretion then raises the ice fractions of the rocky bodies (which now have icy material to consume) and lowers the ice fractions of the icy bodies (which previously had mostly icy material available but now find more rocky material in their feeding zone). Since so much material is brought into the 0.05–2 AU zone from outside, this tends to concentrate the resulting planets at high ice fraction with roughly 20–40% of their mass coming from embryos (the median embryo mass fraction is 0.28). Almost all objects with very low embryo mass fraction ( $< 0.2$ ), which therefore consumed almost all of their material in planetesimals, have very high ice fraction. These values may be biased somewhat by our choice of inner edge, which artificially depletes the innermost regions of rocky planetesimal material.

In the innermost regions,  $a < 0.25$  AU, somewhat counter-intuitively, we find smaller bodies with higher ice content. All objects save one (an  $0.43 M_{\oplus}$  ice-free object from S28A) had masses  $1 M_{\oplus} < M < 4 M_{\oplus}$ , and were composed of at least 50% ice. Excluding the rocky outlier, the median ice fraction was 0.69. Since the maximum ice fraction possible in our simulations is 0.75, these objects are

**Figure 12.** Ice fraction versus amount of material consumed by an object in the form of an embryo (as opposed to a planetesimal). By construction all objects have ice fractions  $\leq 0.75$ .



composed almost entirely of material from beyond the snow line.

### 4.3 Simulation statistics

Chambers (2001) (§4, which we follow closely here) introduced a useful set of dimensionless statistics for comparing the results of terrestrial planet simulations, but as he notes they are of general applicability. (Given our inability to build planets larger than  $8 M_{\oplus}$ , the statistics are rather more closely applicable than we had hoped.) His set includes:

- (i)  $N$ , the number of bodies (here planets).
- (ii)  $S_m$ , the fraction of the total mass in the largest object.
- (iii)  $S_s$ , a spacing statistic, loosely related to the empirical instability time-scale (Chambers et al. 1996; see also Iwasaki & Ohtsuki 2006 for a more recent investigation of the problem, which suggests that the dependence on the mass should be closer to  $0.29 \simeq 2/7$ ), defined by

$$S_s = \frac{6}{N-1} \left( \frac{a_{\max} - a_{\min}}{a_{\max} + a_{\min}} \right) \left( \frac{3M_{\odot}}{2\bar{m}} \right)^{1/4} \quad (17)$$

where  $a_{\min}$  and  $a_{\max}$  are the limiting semimajor axes (here set to 0.05 AU and 2.0 AU), and  $\bar{m}$  is the mean planet mass.

- (iv)  $S_d$ , the normalized angular momentum deficit, defined by

$$S_d = \frac{\sum m_j \sqrt{a_j} (1 - \sqrt{1 - e_j^2 \cos i_j})}{\sum m_j \sqrt{a_j}} \quad (18)$$

with summation over the planets, indexed by  $j$ . (See, e.g., Laskar 1997.)

- (v)  $S_c$ , a concentration statistic, given by

$$S_c = \max \left( \frac{\sum m_j}{\sum m_j [\log_{10}(a/a_j)]^2} \right) \quad (19)$$

where we take the maximum value the argument reaches over all values of the variable  $a$  in the interval [0.05 AU, 2 AU]. The higher the value, the more ‘concentrated’ the

**Table 3.** Summary statistics for each run; definitions as in §4.3. For comparison, the label ‘‘TERR’’ describes the four terrestrial planets in our own system, and 3NEP the three Neptunes in the HD69830 system. Undefined values are labelled N/A, and unknown values left blank. Simulations S21A, S35A, and S37A resulted in no planets interior to 2 AU, and so are not listed.

Sim.	N	$M_{\text{tot}}$	$\bar{m}$	$S_m$	$S_s$	$S_d$	$S_c$	$S_r$
S01A	3	1.50	0.50	0.55	90.23	0.008	73.55	0.44
S01B	4	1.51	0.38	0.31	64.54	0.003	79.20	0.46
S02A	2	3.12	1.56	0.59	135.79	0.014	51.42	1.35
S03A	5	2.06	0.41	0.33	47.35	0.002	84.02	0.59
S03B	2	1.90	0.95	0.80	153.74	0.018	53.78	0.97
S04A	1	4.06	4.06	1.00	N/A	0.016	N/A	2.54
S05A	2	3.78	1.89	0.54	129.43	0.022	35.04	1.49
S05B	3	4.20	1.40	0.39	69.73	0.005	43.67	1.51
S06A	3	9.61	3.20	0.51	56.71	0.007	48.89	3.05
S07A	6	5.17	0.86	0.40	31.49	2.1e-04	23.62	2.99
S07B	2	5.62	2.81	0.63	117.20	0.014	33.75	2.31
S08A	8	5.56	0.69	0.22	23.74	4.5e-05	7.67	10.02
S09A	1	7.19	7.19	1.00	N/A	0.023	N/A	3.49
S09B	8	9.78	1.22	0.23	20.61	1.4e-04	20.13	2.10
S10A	7	7.84	1.12	0.30	24.58	1.1e-04	4.10	10.65
S10B	6	5.12	0.85	0.21	31.57	2.6e-05	27.84	3.07
S11A	2	0.97	0.48	0.58	181.97	9.4e-07	544.68	3.44
S12A	5	4.98	1.00	0.40	37.97	3.8e-04	84.87	1.94
S12B	4	4.42	1.10	0.36	49.33	0.001	75.57	1.83
S13A	5	14.92	2.98	0.34	28.86	9.4e-05	23.58	5.62
S14A	2	5.92	2.96	0.60	115.67	0.007	88.91	2.82
S14B	6	9.67	1.61	0.20	26.93	6.2e-04	36.31	2.73
S15A	6	15.16	2.53	0.25	24.07	0.007	6.86	16.94
S16A	4	10.29	2.57	0.42	39.93	2.7e-04	54.90	2.53
S16B	4	16.75	4.19	0.37	35.35	0.012	21.20	3.39
S17A	5	8.47	1.69	0.44	33.25	2.1e-04	2.21	30.17
S17B	2	11.36	5.68	0.56	98.28	0.041	13.34	6.12
S18A	2	1.01	0.50	0.67	180.19	5.0e-07	32.16	3.74
S19A	6	6.02	1.00	0.21	30.32	1.0e-06	6.10	14.58
S19B	2	2.05	1.03	0.52	150.72	9.3e-06	1426.51	11.62
S20A	3	5.42	1.81	0.38	65.44	2.7e-06	25.43	33.28
S22A	1	3.33	3.33	1.00	N/A	2.4e-06	N/A	2.05
S23A	3	1.12	0.37	0.67	96.94	0.002	122.19	0.23
S24A	3	1.27	0.42	0.41	93.96	0.034	42.33	0.45
S25A	3	2.30	0.77	0.42	81.07	0.002	94.80	0.67
S26A	2	2.80	1.40	0.64	139.49	0.011	70.28	1.32
S27A	5	4.89	0.98	0.37	38.14	0.001	50.19	1.28
S28A	9	7.42	0.82	0.15	19.90	2.1e-04	11.39	2.70
S29A	3	3.42	1.14	0.43	73.39	6.3e-04	119.09	1.36
S30A	3	5.42	1.81	0.65	65.42	9.7e-04	79.77	1.89
S31A	5	10.65	2.13	0.35	31.40	1.4e-04	47.78	2.35
S32A	4	7.00	1.75	0.34	43.97	0.002	9.02	7.42
S33A	3	7.85	2.62	0.66	59.65	0.007	45.37	3.39
S34A	5	4.16	0.83	0.38	39.71	2.2e-04	19.50	6.39
S36A	1	3.92	3.92	1.00	N/A	6.6e-05	N/A	2.29
TERR	4	1.98	0.49	0.51	6.29	0.002	89.49	
3NEP	3	41.00	13.67	0.45	4.12	0.004	7.05	

radial distribution is, although this statistic is not a proxy for the mass surface density.

- (vi)  $S_r$ , a radial mixing statistic, given by

$$S_r = \frac{1}{\sum m_j} \sum \frac{m_j |a_{j,0} - a_{j,f}|}{a_{j,f}} \quad (20)$$

where 0 and  $f$  refer to the original (at  $t=0.4$  Myr) and final (at  $t=100$  Myr) semimajor axes of each object which ultimately becomes part of one of the resulting planets. This statistic was introduced in Chambers (2001) to quantify the degree of mixing induced by gravitational scattering. Being linear in the change in semimajor axis, this statistic may not prove as useful measuring this effect in simulations with high migration rates, but will quantify the degree of type I migration instead.

These statistics, along with the total mass  $M_{\text{tot}}$  and mean mass  $\bar{m}$ , are listed in table 3, as well as the corresponding values for our terrestrial system (Mercury, Venus, Earth, and Mars) and the system of three Neptune analogues orbiting HD69830.

#### 4.3.1 Final number of planets and radial mixing

A somewhat surprising outcome of the simulations is that there were so many systems with high  $N$  which survived: 9 of the 48 simulations resulted in systems with  $N > 5$  even after 100 Myr. Some of this surprise is explained by the fact

that intuitions trained on the terrestrial regime can fail for  $a < 0.5$  AU, where the same radial separation corresponds to a much greater Hill separation, and many of the high- $N$  systems have multiple objects in the interior. Removing these objects from consideration reduces the number of high- $N$  systems to 5. That said, these systems (both the original 9 and the reduced 5) cover every  $\alpha$ , include  $f_{\text{enh}} = 3$  and 5, both  $\tau_{\text{decay}}$  values, both  $S_{\text{loc}}$  values, and all but one have  $c_a = 1.0$ . This ubiquity suggests that the unexpectedly large number of planets is likely to be the result of strong migration selecting stable configurations.

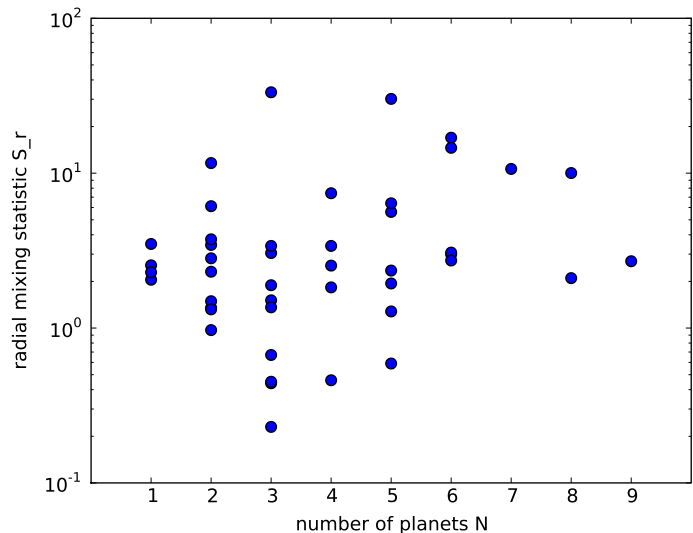
When applied to our runs, the radial mixing parameter  $S_r$  defined by equation 20 provides a measure of the degree of migration experienced by all components of the final planetary system. For example, a (somewhat unrealistic) system of two equal mass planets which begin life with semimajor axes  $a \simeq 2$  AU, and subsequently migrate inward without further accretion to the radial distance  $\simeq 0.2$  AU will have a value  $S_r \simeq 10$  (this value becomes  $S_r \simeq 20$  if the final stopping location decreases to 0.1 AU; it becomes  $S_r = 1$  if the final stopping distance increases to 1 AU). As figure 13 shows, while there are many low- $N$  runs with  $S_r$  comparable to the high- $N$  values, there are no high- $N$  runs with low  $S_r$ . Of the 9  $N > 5$  runs, all had radial mixing  $S_r > 2$ , with 4 having  $S_r > 10$  (44%); of the 40  $N \leq 5$  runs, 40% had  $S_r < 2$ , and only 3 had  $S_r > 10$  (7%). This suggests – albeit weakly, given the small numbers involved – that high- $N$  systems consist of bodies that formed over a wide range of radii and migrated into the interior region. There are also no high- $N$  runs with  $M_{\text{tot}} < 5 M_{\oplus}$  (numerous planets add up to a significant amount of total mass). The absence of any high- $N$  systems with  $f_{\text{enh}} = 10$  is likely the result of the would-be planets migrating out of our integration region, and another example of how in this regime higher surface densities can hurt more than they help. Indeed, all three runs which resulted in no planets interior to 2 AU (S21A, S35A, and S37A) all had  $f_{\text{enh}} = 10$  and  $c_a = 1$ , although here our choice of outer boundary may be playing a role; we return to this issue in §5.1.

It is probable that the perturbations from giant planets would significantly lower these numbers. Their formation is not modelled here: accretion of gas is not treated, nor are any objects of  $a > 2$  AU after 6 Myr. Chambers (2001) notes that one explanation consistent with the observed decrease in terrestrial planet number between his simulations and those of some previous authors was his incorporation of the Jovians, and a similar effect should occur here. McNeil et al. (2005) also had to invoke an external random velocity source to reduce the number of planets in late-stage prototerrestrial systems produced via oligarchic migration. Of course, even had we incorporated a gas accretion model, we do not form any objects large enough to serve as useful seeds for the Pollack et al. (1996) picture while the gas is present.

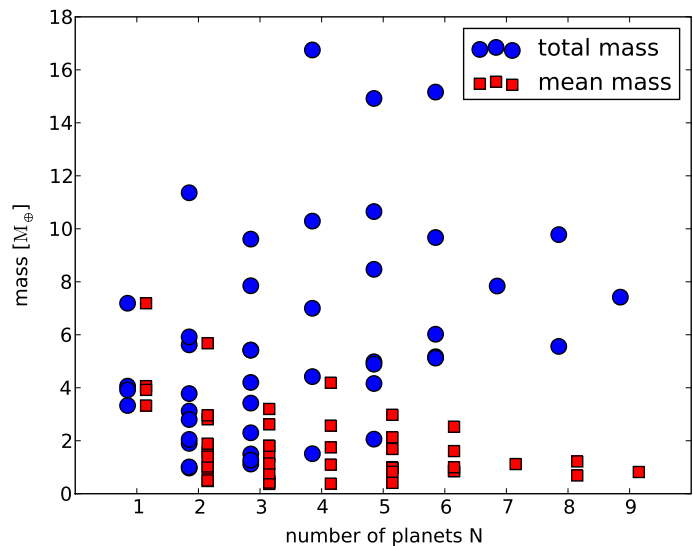
#### 4.3.2 Total surviving mass

Of primary importance for our purposes is the total amount of mass which survives interior to 2 AU at  $t=100$  Myr. Only 6 runs succeeded in producing more than  $10 M_{\oplus}$  of material inside 2 AU. Despite the small number, it is striking that every one had  $f_{\text{enh}} = 5$  and  $S_{\text{loc}} = 2.7$  AU, with  $\alpha < 1.0$ . S16 – with  $\alpha = 0.5$ ,  $c_a = 0.3$ ,  $\tau_{\text{decay}} = 1$  Myr – was particularly

**Figure 13.** Number of planets versus radial mixing parameter.

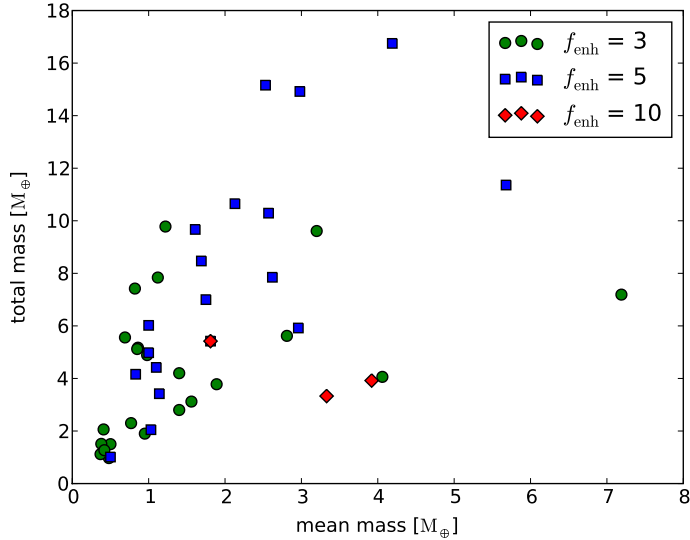


**Figure 14.** Number of planets versus total and mean planet mass.



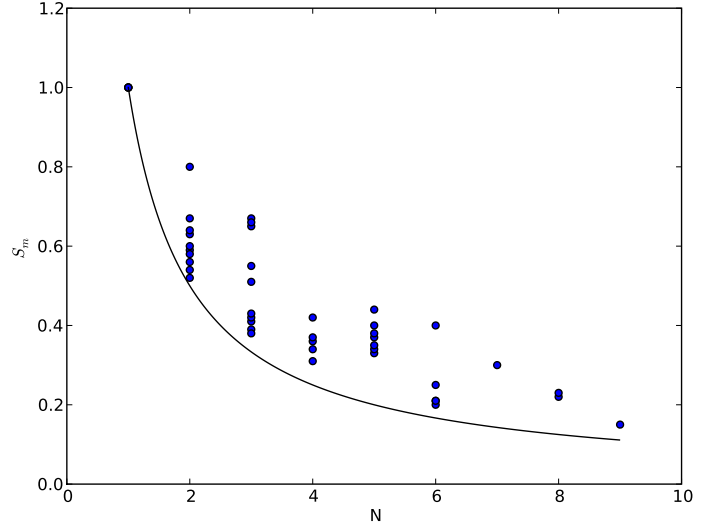
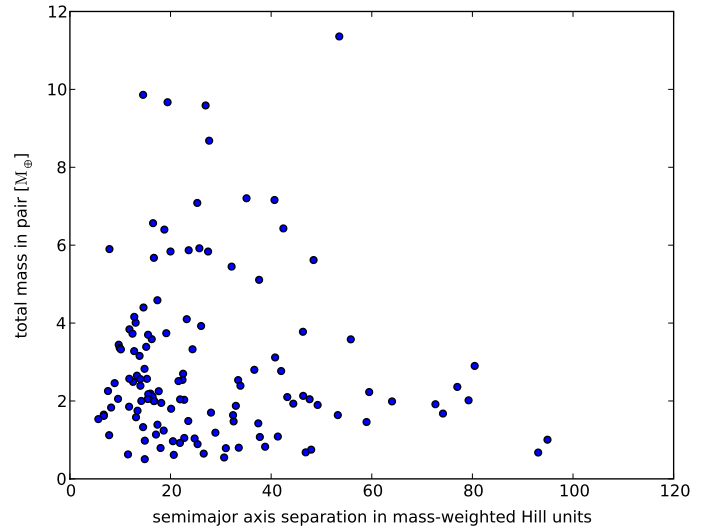
successful, with both instantiations producing over  $10 M_{\oplus}$ , and S16B producing two of the largest bodies in the suite and the single largest total mass,  $16.75 M_{\oplus}$ . Recall that for our vertical profile (eq. 3),  $\alpha = 1.0$  is the transition between convergent and divergent migration for equal-mass bodies, and that for  $\alpha < 1.0$ , neighbouring equal-mass migrating objects converge. At the outset of this project we had hoped that the compression might increase the resulting masses, and both the behaviour at the high  $M_{\text{tot}}$  limit and summing over the other parameters as in table 2 support this hope. When the  $M_{\text{tot}}$  limit is lowered to  $5 M_{\oplus}$ , 7 of the 23 runs (30%) had  $\alpha = 1.0$ , and so any advantage that convergent values of  $\alpha$  possess seems limited to the extremes (which is where one might expect to first observe increases in the variance of the mass with a lowered  $\alpha$ .)

Figure 14 shows the variation of  $M_{\text{tot}}$  and  $\bar{m}$  with

**Figure 15.** Total mass versus mean mass.


the number of planets. The cluster of high-mass runs with  $M_{\text{tot}} \gtrsim 15 M_{\oplus}$  had nearly the median number of planets ( $4 \leq N \leq 6$ ), while both lower and higher values of  $N$  had lower maximum  $M_{\text{tot}}$  ( $11.4 M_{\oplus}$  and  $9.8 M_{\oplus}$ , respectively). This hints that median  $N$  values produce the largest masses, but there are only three high-mass runs involved. Moreover, the four runs with  $N > 6$  also have mean and median  $M_{\text{tot}}$  greater than or comparable to the median runs, even if the maximum is greatly reduced (unsurprisingly, having more planets tends to translate into a greater total mass). It does appear that both the maximum value and the variance decrease with small and large  $N$ ; there are no runs with  $N \geq 6$  and  $M_{\text{tot}} < 5 M_{\oplus}$ . There is also a strong correlation between the number of resulting planets and their mean mass, such that the larger  $N$  is, the lower  $\bar{m}$  is. The curves which bound  $\bar{m}$  as  $N$  varies are quite regular, which given the volume of parameter space that our search covered is strong evidence that we must make large modifications to our initial conditions or our physics to increase  $\bar{m}$  to Neptune-like masses at  $N \geq 3$ .<sup>3</sup>

One way to see the difficulty is to compare the total mass in a run with the mean mass (fig. 15; zero-mass outcomes are suppressed.). There is a cluster of very low-mass runs with  $\bar{m} \sim 0.5 M_{\oplus}$ , but at larger  $\bar{m}$  and  $M_{\text{tot}}$  the region of achieved values opens up. Clearly  $\bar{m} \leq M_{\text{tot}}$ , which sets the lower boundary curve. Removing the high- $\bar{m}$  outliers, the  $f_{\text{enh}} = 3$  and  $f_{\text{enh}} = 5$  cases show similar behaviour, except that the  $f_{\text{enh}} = 5$  set reaches higher total masses and has a larger variance. Not only do the  $f_{\text{enh}} = 10$  cases fail to improve on the  $f_{\text{enh}} = 5$  case, each is inferior to many  $f_{\text{enh}} = 3$  runs. Worse yet, three zero-mass runs were not plotted, although some of those had full migration and lost implausible amounts of mass to the star. This leads us to tentatively conclude that any mechanism that increases

**Figure 16.** Number of planets versus fraction in largest body. The line corresponding to  $1/N$  is plotted.

**Figure 17.** Mass and separation of neighbouring pairs at  $t=100$  Myr.


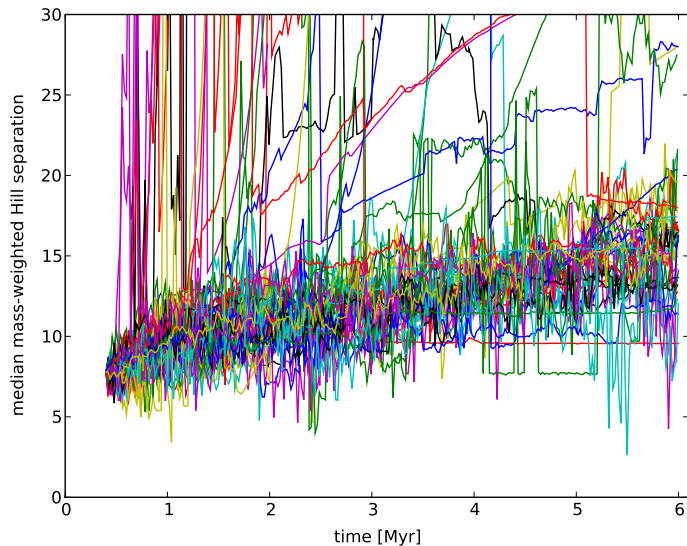
the rate of planetary growth during early times is likely to reduce, and not increase, the mass of the largest surviving bodies in the presence of significant inward type I migration.

Figure 16 shows the fraction of the total mass contained in the largest body (by definition, this cannot be smaller than  $1/N$ ). Slightly under half of the planet-producing simulations have  $S_m > 0.5$ , and the trend toward lower  $S_m$  with larger  $N$  is clear. For comparison, the current HD69830 value has  $N = 3$ ,  $S_m = 0.45$ , well within the achieved range.

#### 4.3.3 Future mergers and long-term stability

It is unlikely that most of the resulting systems will undergo many more mergers (save S24A). Figure 17 shows the mass in each pair of neighbouring planets in all the resulting systems against the mass-weighted Hill separation

<sup>3</sup> It is darkly amusing to note that naively extrapolating the best fit line for the maxima predicts that the desired  $\bar{m} \simeq 15 M_{\oplus}$  occurs at  $N \simeq -11$ , a situation which should defeat even the admirability of today's observational exoplanetary community.

**Figure 18.** Evolution of median separation of planets interior to 2 AU.

( $\bar{b} = ((M_1 + M_2)/3M_\odot)^{1/3}(M_1a_1 + M_2a_2)/(M_1 + M_2)$ ) of the pair. There are only 5 pairs of planets involving total masses greater than  $8M_\oplus$ , and 4 of those have  $\bar{b} \gtrsim 20$ . The median  $\bar{b}$  is  $\simeq 22$ , and the median mass of objects closer than the median separation is only  $2.3M_\oplus$ . If we follow the mass-separation relationship for each pair through the simulations, we find that the vast majority of pairs which have small separations have combined masses  $< 4M_\oplus$  (which helps explain why we do not form very many large objects).

Figure 18 shows the evolution of the median mass-weighted Hill separation of all objects inside 2 AU for all simulations until 6 Myr. While the data are quite noisy, it is clear that almost all simulations show a definite evolution from their initial value of  $\simeq 7$  ( $\simeq 9$  in single-planet units) to  $\simeq 15$  ( $\simeq 19$ ); the median outcome is 16.5. 33 of the 48 simulations (69%) have median  $\bar{b} > 15$ , and 14 have median  $\bar{b} > 20$ . Only 6 of the runs (12.5%) had median  $\bar{b} < 13$ . This difference can be significant as the interaction time-scale is a strong function of the separation. Work by Iwasaki & Ohtsuki (2006) shows that the time-scale for a collection of cold equal-mass objects to suffer an instability in the absence of nebular gas when separated by 15–20 mutual Hill radii can be  $> 10^{10}$  years. These systems have much shorter interaction times in practice due to the variance of the spacing and the nonzero eccentricities (Zhou et al. 2007), but the likelihood of the set of planets merging to form Neptune-sized objects even when the total mass makes it possible is very low. In any case, these total masses are far beneath the  $\sim 41M_\oplus$  present in the HD69830 system, and the maximum mass of  $7.19M_\oplus$  is far below the estimated  $18.4M_\oplus$  of HD69830 d.

## 5 DISCUSSION

### 5.1 Weaknesses of the model

As usual, many of the approximations invoked to make the simulations tractable may have affected the results.

The semianalytic model used to advance the early stages of the model is quite primitive. It uses a fixed Hill spacing of 10 between the embryos, using neither the original Kokubo & Ida (1998) dependence of  $b$  on  $M$  nor a more realistic slower growth. This should be a tolerable error during the first 0.5 Myr for all but the highest-enhancement cases. The approximation of the embryo distribution by a smooth function means that most of the interembryo dynamics is lost, which can be important when tidal convoys of migrating objects locked into mean-motion resonance form. In a noisy N-body migration problem, objects which become larger than their neighbours due to a merger can push interior embryos with it at migration rates larger than the naive model would predict (as in S07A – see figure 2). Chambers (2008) discusses this issue in the context of building semi-analytic models of oligarchy. The use of a large seed mass  $M_0$  makes the discs easier to instantiate in the N-body code by lowering the gradient in embryo mass, but at the cost of artificially accelerating the growth of the most distant objects, which should lead to higher migration. Quite substantial growth above this initial mass is required, however, to enable trans-snowline embryos to migrate interior to 2 AU, so this is unlikely to be a significant problem in the simulations.

Enforcing a sharp embryo/planetesimal distinction such that planetesimals neither self-gravitate nor accrete, the usual procedure in the field among those using Kepler-problem symplectic integrators, results in a poor treatment of the mass spectrum. No planetesimals can promote themselves to embryos, even if a planetesimal ring forms in which the largest body should experience runaway growth and become a new oligarch. This will suppress embryo growth in some cases (when an oligarch should have formed), and increase it in others (by providing a fresh supply of material for protoplanets migrating into the region to consume, as in Tanaka & Ida 1999 and the models of Alibert et al. 2006). The use of a uniform characteristic planetesimal radius means that we are insensitive to the differing effects of aerodynamic drag on different-sized objects. While the planetesimal non-accretion problem is difficult to overcome, the uniform-mass problem could be handled by varying the radius assigned to super-planetesimals, so that some objects would trace the behaviour of 1 km bodies, some 10 km, and so on. However, in the absence of any collisional physics – here, we use a simple hit-and-stick model with no fragmentation – the small-radius planetesimals will not be replenished as they would be in a real system. The absence of a collisional cloud may increase the eccentricity of the resulting planets as an object cannot be damped by its own debris, but this is probably negligible during the gas-rich phase when type I drag is strong and the embryos are on effectively circular orbits the majority of the time.

Ultimately, it will be necessary to use a hybrid N-body/statistical scheme along the lines of Bromley & Kenyon (2006), and we are currently exploring the incorporation of a variant of the semianalytic model of Chambers (2008) into the code.

The choice of inner and outer edge for the initial solid material distribution in the N-body runs – 1.0 AU and  $\sim 10$  AU – may have changed the outcomes in two ways. In the runs with low migration, some objects which should have been present in the interior will be missing. However, this



is seldom a significant amount of mass. The only disc in which there was more than  $4M_{\oplus}$  of material interior to 1 AU which was excluded was the  $f_{\text{enh}} = 10, \alpha = 1.0$  case ( $\sim 8M_{\oplus}$ ), which has very high migration; S22A, S36A, and S37A all fail to contain any objects inside of 1.5 AU because they have all migrated away, and so very little material (if any) would have survived. In the discs with the lowest migration rates, where  $f_{\text{enh}} = 3$ , only  $2.3M_{\oplus}$  of mass was missed when  $\alpha = 1.0$ . (The flatter profiles have more of their mass at larger  $r$  and so have even less initial mass inside of 1 AU.) Therefore the effects on the final results are limited: low-enhancement discs which have migration rates small enough that we should have included the innermost embryos also have too little mass in the region to be interesting, and high-enhancement discs which have enough mass to significantly affect the mass of a final planet have migration rates high enough that the missing material is long gone by the time the gas disc has dissipated. The inner cut-off edge of 0.05 AU will also be responsible for removing some particles with small semimajor axis and high eccentricity, but there are very few of them. On the outer edge, it is quite possible that a wider particle disc than 10 AU would have resulted in more planets in the high-enhancement runs and prevented the zero-planet outcomes (all of which were very high-migration configurations with  $f_{\text{enh}} = 10$  and  $c_a = 1$ ). However, such high enhancements and migration rates are at the limits of plausibility to start with, and the initial conditions from the semianalytic model are questionable at high  $f_{\text{enh}}$ . Most importantly, there is no reason to expect that the planets which would have been formed would be any larger than the ones already formed in the  $f_{\text{enh}} = 10$  runs, as objects which migrate into the inner regions in such runs are often either well-separated or resonantly locked and therefore protected against most encounters.

In our N-body model, the only effect that the gas disc has upon the particles is via prescription as a source of drag, whether aerodynamic or type I, and we did not include any disc physics involving gap opening. This probably had little effect, as if we assume a (hydrodynamic-standard) constant  $z_0/a$  ratio of  $\simeq 0.05$ , and use the gravitothermal condition from Crida et al. (2006), gap opening even in an inviscid disc requires  $(3/4)(z_0/r_H) < 1$ , or  $r_H \simeq 3/4H$ , which gives a mass of  $\simeq 53M_{\oplus}$  (with "gap opening" defined to be a 10% perturbation in surface density). Even assuming a ratio of  $1/2$  sufficed to open a gap, we would need  $\simeq 17M_{\oplus}$ . Things become somewhat better in a flared disc (such as the one we actually used) with  $z_0/a \propto a^{1/4}$ , where if we assume no kinematic viscosity, an  $8M_{\oplus}$  object could possibly start opening a gap at  $\sim 0.08$  AU, near the edge of our simulation region. In practice, gap opening is unlikely to be a good explanation for the presence of the 'lukewarm' end of the hot Neptune population unless it is substantially more efficient than currently thought.

We also neglected the accretion of gas onto the embryo cores. Given the low planet masses we obtained – with median  $1M_{\oplus}$  and maximum  $\simeq 8M_{\oplus}$  – the standard Pollack et al. (1996) model suggests that even our most massive planets would have accreted atmospheres of at most  $1\text{--}2M_{\oplus}$ . This missing mass should not have affected the outcomes significantly, at least directly, as it would have changed the Hill radii by less than 10%. However, it is known (Inaba & Ikoma 2003) that growing embryos can have a sig-

nificantly increased effective capture radius due to the energy loss suffered by planetesimals moving through the embryo atmosphere, which can help overcome the challenge of forming giant planet cores before the gas disc evaporates (Inaba et al. 2003). Would including this effect have made it possible to form substantially larger cores?

This question should be considered in a larger context. One feature common to many of the new mechanisms being discussed, atmosphere-enhanced capture radii included, is that they tend to increase the accretion rate at early times. Partly this is due to a target bias on the part of scientists studying the middle and late stages of planet formation, as forming the cores of giant planets on appropriate time-scales is an important open problem even in the migration-free case, and so efforts have been concentrated in the direction of making large objects easier to form. In the absence of migration, this is a net positive. The situation is more complicated when migration is involved. Increasing the accretion rate sounds appealing, but since the type I migration rate scales linearly with the mass, it will simultaneously decrease the migration time-scales, and do so at early times when the gas density is at its highest. If anything, this will make the formation-to-migration time-scale problem worse, at least in cases where migration is significant. Daisaka et al. (2006) noted that for a fixed gas-to-dust ratio and gas dissipation time-scale, increases in initial surface density can result in decreases in final surface density. Chambers (2008) finds that for a disc with alpha viscosity of 0.001, the maximum embryo mass increases as the disc mass increases to a high of  $\simeq 3M_{\oplus}$  at  $0.05M_{\odot}$ , and then falls off, so that disc masses of  $0.03M_{\odot}$  and  $0.07M_{\odot}$  both have maximum planet mass  $0.5\text{--}0.6M_{\oplus}$ . Including fragmentation does raise the maximum mass reached over a wide range of disc mass ( $0.03\text{--}0.10M_{\odot}$ ), but only to  $\simeq 4M_{\oplus}$ . The case with alpha viscosity of 0.01 resembles the case without migration below disc masses of  $0.05M_{\oplus}$ . Only at very large disc masses, greater than  $0.10M_{\odot}$ , are Neptune-like masses recovered.

Modifying the accretion rate seems unlikely to encourage neighbouring oligarchs to merge at late times, given their large separations. These spacings are consequences of the high surface density of the discs as well as type I migration. Enhanced capture radius mechanisms should have little direct effect on the giant impact phase, as a body needs to encounter roughly its own mass of gaseous material in the extended atmosphere to significantly affect its orbit. For example, Earth-mass objects experiencing a near-collision will barely notice any atmosphere, however extended. In general, changes to the accretion rate in these oligarchic migration scenarios should move the window of source material which grows and migrates to the innermost regions, but will not increase the total mass by the factors of several needed to recover a planetary system resembling HD69830 (except possibly for massive discs). That is, it should change where the planets come from, not how large they are.

## 5.2 Comparisons with previous work

Our results differ significantly from previous results in the literature, chiefly in that we fail where they succeed.

Alibert et al. (2006) succeeded in forming a system which resembles the HD69830 system very closely, by reducing the strength of the migration by a factor of 10

and considering only three cores which migrate and accrete (c.f. Tanaka & Ida 1999). As Chambers (2008) explains, the presence of interior embryos with a much shorter dynamical time means that inward-migrating cores do not encounter a pristine feeding zone, but one which is already substantially processed. None of our migrating cores experienced growth resembling that in the Alibert et al. (2006) model. Payne et al. (2009) further find that aerodynamic drag can significantly decrease the planetesimal accretion rate in such scenarios, keeping the migrating core acting as a shepherd and not a predator.

An alternative way of ensuring that a population of hot super-Earths or hot Neptunes can form and survive is to invoke an inner disc cavity generated by interaction between the disc and the stellar magnetosphere. Such a model has been used to explain the existence of hot Jupiters (Lin et al. 1996), and was incorporated into the formation models of Brunini & Cionco (2005) and Terquem & Papaloizou (2007) (who also included tidal interaction with the central star). Brunini & Cionco (2005) and Terquem & Papaloizou (2007) both succeeded in forming large short-period Neptune-mass ( $10\text{--}30 M_{\oplus}$ ) cores. Terquem & Papaloizou (2007) form four objects of mass  $\geq 8M_{\oplus}$ , the largest being  $12M_{\oplus}$ , and Brunini & Cionco (2005) form five objects of mass  $\geq 10M_{\oplus}$ , with the largest being  $\sim 24M_{\oplus}$ . There are three main differences between their models and ours which likely account for the discrepancy. First, both are relatively low-resolution: Terquem & Papaloizou (2007) used only 10 Earth-mass bodies in all but one of their runs, and Brunini & Cionco (2005) used 100 embryos of  $0.5 M_{\oplus}$  and 200 planetesimals of  $0.1 M_{\oplus}$ . Second, and more importantly, it is unlikely that their initial masses and spacings can be recovered from a self-consistent oligarchic migration model: there is no plausible prior configuration which would evolve into (for example) 12 Earth-mass bodies spaced between 0.1 and 1 AU. Finally, and most importantly, in accordance with the cavity hypothesis both groups used a disc with an inner edge at either 0.05 AU or 0.10 AU, and we did not. Some small toy simulations we performed (unpresented here) confirm that we can also build bodies of  $\simeq 15M_{\oplus}$  by doing so, but only relatively close to the boundary. However, from general considerations the magnetospheric cavity in this model is expected to extend out to a distance of  $\simeq 0.08$  AU for an assumed T Tauri star rotation period of 8 days (Lin et al. 1996), causing migration to halt at a distance of  $\simeq 0.05$  AU from the star. We simply note that there are a number of super-Earths and Neptune-mass extrasolar planets orbiting with significantly larger semimajor axes (e.g. HD69830 d, or OGLE-05-169L b, at 2.8 AU) whose inward migration was probably not halted by the presence of an inner disc cavity. It is more likely that they, or their progenitor objects, were stranded at or near their current location when the gas disc dispersed.

Thommes et al. (2007) and Chambers (2008) use semi-analytic models, both incorporating atmosphere-enhanced capture radii and the latter fragmentation, and succeed in forming planets of  $\geq 10M_{\oplus}$ , although Thommes et al. (2007) produce far more than Chambers (2008). They both use an approach in which embryos are treated as discrete but non-interacting objects instead of as a continuous distribution (replacing the more Eulerian treatment of Thommes et al. 2003 and Chambers 2006 with a Lagrangian

one). In order to maintain the standard oligarchic separation of  $\sim 10$  Hill radii, they merge two embryos whenever their semimajor axes differ by less than 7 Hill radii. As Chambers (2008) notes, this will result in missing some interesting inter-embryo dynamics such as migration convoys (groups of embryos migrating in mean-motion resonance, as in McNeil et al. 2005; see also Thommes 2005; Papaloizou & Szuszkiewicz 2005), but it will also miss some larger and more fundamental dynamics such as deviations of the embryo behaviour from the semianalytic predictions, and introduce an unphysical orderly merger wave.

Chambers (2008) performed a comparison between the results of his semianalytic model and one of the terrestrial-planet N-body integrations of McNeil et al. (2005), and found that the N-body results had both larger median masses ( $0.25M_{\oplus}$  vs.  $0.16M_{\oplus}$ ) and larger median spacings ( $\sim 20$  Hill radii vs. 11). Even in the original oligarchic model of Kokubo & Ida (1998), there is a weak dependence of  $b$  on  $M$  and  $\Sigma$ . If in these scenarios the interembryo spacing grows to values much larger than 10 while the objects stay on near-circular orbits, oligarchic growth can be quenched (e.g. Iwasaki & Ohtsuki 2006; Zhou et al. 2007). As Chambers (2006) (§8) notes, in order to maintain a constant spacing in  $b$  within a fixed width, embryos must accrete  $1/3$  of their mass via embryo-embryo mergers. This accretion mode should vanish if the embryos are too well-separated (and too cold, but the models assume the embryos are always on circular orbits.) Too large a spacing towards the end of the gas phase can also suppress the giant-impact phase almost entirely, requiring external sources of stirring to form large cores on reasonable time-scales. Accordingly, if the interembryo spacing  $b$  for large-mass bodies in these simulations is closer to 15–20 than 10, then calibrating the (admittedly merely statistical) prescription for the embryo mergers to the no-migration, low-embryo-mass separation value of 10 may not be appropriate.

Despite the differences, we find some qualitative agreements with Chambers (2008). In his models with migration but without fragmentation (the closest match to our runs), he finds that the maximum mass of an object is maximized at  $\simeq 3M_{\oplus}$  for a disc mass of  $0.05M_{\odot}$ , and that both higher and lower disc masses decrease this number (as we find, and Daisaka et al. 2006 predicted). For his simulations which include both fragmentation and migration, as mentioned above, there is a wide range of disc masses ( $0.03\text{--}0.10M_{\odot}$ ) which produce roughly comparable maxima ( $\simeq 4M_{\oplus}$ ). The only simulations which succeed in getting cores larger than  $10M_{\oplus}$  either fail to include migration or include both fragmentation and migration with a disc mass of  $\gtrsim 0.1M_{\odot}$ , and it appears that the only Neptune-like object had a semimajor axis outside 2 AU. This is in mild disagreement with Thommes et al. (2007), who found  $10 M_{\oplus}$  objects were common, which Chambers (2008) argues is the result of their choices of a large alpha viscosity, 0.01, and a small planetesimal radius, 1 km, while neglecting fragmentation.

We suspect that the solution to the short-period Neptune formation problem lies not in tweaking the accretion rate but in modifying the prescription for the interaction with the gas disc. Obviously we need some kind of migration to build a short-period population, but what properties should it have? Ideally, we would prefer a migration which: (1) has little to no effect at early times when the gas density

is high, so that enhancing the surface density actually results in larger embryos and not more embryos lost, (2) when active, has a reduced rate from the nominal Tanaka et al. (2002) behaviour, as our  $c_a = 0.3$  runs performed noticeably better than our full migration runs, and (3) provides some mechanism to encourage large migrating embryos to merge instead of locking in convoys or stranding themselves at large separations from their neighbours, such as a variable migration direction.

The most promising model of disc-induced migration which displays these characteristics is that presented by Paardekooper & Mellema (2006, 2008), in which the migration of planets in radiatively inefficient discs was considered. This model has the highly desirable property that migration is stopped, or even reversed, during early times when the disc is optically thick, but inward type I migration is recovered when the disc density decreases and the gas becomes optically thin. An alternative model for the modification of type I migration is stochastic migration induced by turbulent density fluctuations in the disc (Nelson & Papaloizou 2004; Nelson 2005). Although this does not appear to have the same nicely-tailored characteristics for solving the problem of short-period Neptune formation as the radiatively inefficient migration model, its random walk nature has the potential to deliver significant planetary material into the interior regions at late times.

## 6 CONCLUSIONS

We performed 48 simulations of various oligarchic migration scenarios to determine whether the simplest standard approach can succeed in forming a population of short-period Neptune systems under common assumptions for the protoplanetary disc parameters. Multiple numerical techniques were applied: semianalytic techniques for the first 0.4 Myr, our new parallel multizone N-body code for the accretion phase while gas is present up to 6 Myr, and the more traditional SyMBA approach for the late stage to 100 Myr.

We find that over a wide range of disc conditions, it is difficult to form planets of mass greater than  $3 - 4M_{\oplus}$ . Our most successful runs involved  $\sim 5$  times the mass of the MMSN, surface density varying as  $r^{-1/2}$ , a disc decay time-scale of 1 Myr, and a migration efficiency of 0.3. Our most common planet outcomes are of Earth-mass objects, with the terrestrial planets having ice fractions from 0.0 to 0.75 (the maximum possible in our simulations). The larger objects have higher ice fractions, with the median being 0.60 for objects above  $1 M_{\oplus}$ , and 0.36 below. In none of the cases did we succeed in forming an object of greater than  $7.5 M_{\oplus}$  inside 2 AU, much less inside 0.5 AU, and the total embryo mass remaining inside 2 AU was always less than  $17 M_{\oplus}$ . The existence of an upper limit and the weak dependence on most parameters is in accordance with the predictions of Daisaka et al. (2006), and in rough agreement with the predictions of Chambers (2008) except at large disc masses. Nevertheless, we should be wary of making predictions based on these results regarding extrasolar planetary systems, as they entirely fail to reproduce the short-period Neptune planetary population that we know exists.

Our failure can be compared to several previous successes in the literature, which either (1) adopt initial con-

ditions which are not easily reconciled with an oligarchic growth picture, (2) use an inner edge to the migration (which is defensible but will have difficulty explaining more distant Neptunes), or (3) neglect inter-embryo dynamics and use an embryo merger condition which is calibrated to an effective inter-embryo separation (10 Hill radii) which is considerably smaller than we observe.

Varying parameters which we kept constant such as the gas-to-dust ratio, incorporating additional accretion physics such as fragmentation, moving to extremely large disc masses or extremely weak migration, and simply performing more runs (and hoping for fortuitous late mergers), could possibly succeed in improving the maximum mass reached by a factor of two and therefore into the Neptune-like region. It seems quite unlikely that they will increase the median mass enough to comfortably produce a population of multiple-planet short-period Neptune systems. We conclude that forming a system like HD69830 will probably require a significant revision to the simple models explored here.

If the standard oligarchy-plus-type-I-migration picture fails to reproduce the observed distribution of short-period exoplanets even at more extreme parameter values, then we must consider non-standard models. Oligarchy is relatively well understood both analytically and numerically; by comparison type I migration is sensitive to poorly understood properties of the gas disc such as disc turbulence and local thermodynamic time-scales. In a follow-up paper we consider the implications for hot exoplanet formation via oligarchy of alternate migration models (such as Paardekooper & Mellema 2006) which show some promise.

## ACKNOWLEDGMENTS

DSM is very grateful for the warm hospitality of Makiko Nagasawa at the Edge Institute at the Tokyo Institute of Technology, where an early version of this work was presented. We appreciate the careful review of the anonymous (but recognizable) referee. The authors gratefully acknowledge the support of SFTC grant PP/D002265/1. The simulations presented in this paper were performed using the QMUL HPC facilities funded through the SRIF initiative, without which the research would not have been possible.

## REFERENCES

- Adachi, I., Hayashi, C., & Nakazawa, K. 1976, *Progress of Theoretical Physics*, 56, 1756
- Alibert, Y., et al. 2006, *Ast. & Astrophys.*, 455, L25
- Andrews, S. M., & Williams, J. P. 2005, *Ap. J.*, 631, 1134
- Andrews, S. M., & Williams, J. P. 2007, *Ap. J.*, 671, 1800
- Bakos, G. Á., et al. 2009, arXiv:0901.0282
- Beichman, C. A., et al. 2005, *Ap. J.*, 626, 1061
- Bromley, B. C., & Kenyon, S. J. 2006, *AJ*, 131, 2737
- Brunini, A., & Cionco, R. G. 2005, *Icarus*, 177, 264
- Bryden, G., Chen, X., Lin, D. N. C., Nelson, R. P., & Papaloizou, J. C. B. 1999, *Ap. J.*, 514, 344
- Butler, R. P., Vogt, S. S., Marcy, G. W., Fischer, D. A., Wright, J. T., Henry, G. W., Laughlin, G., & Lissauer, J. J. 2004, *Ap. J.*, 617, 580

- Chambers, J. E., Wetherill, G. W., & Boss, A. P. 1996, *Icarus*, 119, 261
- Chambers, J. E. 1999, *Mon. Not. R. Astr. Soc.*, , 304, 793
- Chambers, J. E. 2001, *Icarus*, 152, 205
- Chambers, J. 2006, *Icarus*, 180, 496
- Chambers, J. 2008, *Icarus*, 198, 256
- Chiang, E., & Murray-Clay, R. 2007, *Nature Physics*, 3, 604
- Ciesla, F. J., & Cuzzi, J. N. 2006, *Icarus*, 181, 178
- Cresswell, P., & Nelson, R. P. 2008, *Ast. & Astrophys.*, 482, 677
- Crida, A., Morbidelli, A., & Masset, F. 2006, *Icarus*, 181, 587
- Daisaka, J. K., Tanaka, H., & Ida, S. 2006, *Icarus*, 185, 492
- Duncan, M. J., Levison, H. F., & Lee, M. H. 1998, *AJ*, 116, 2067
- Fogg, M. J., & Nelson, R. P. 2007, *Ast. & Astrophys.*, 461, 1195
- Haisch, K. E., Jr., Lada, E. A., & Lada, C. J. 2001, *Ap. J. Lett.*, 553, L153
- Hayashi, C. 1981, *Progress of Theoretical Physics Supplement*, 70, 35
- Inaba, S., & Ikoma, M. 2003, *Ast. & Astrophys.*, 410, 711
- Inaba, S., Wetherill, G. W., & Ikoma, M. 2003, *Icarus*, 166, 46
- Iwasaki, K., & Ohtsuki, K. 2006, *AJ*, 131, 3093
- Levison, H. F., & Duncan, M. J. 2000, *AJ*, 120, 2117
- Lodders, K. 2003, *Ap. J.*, 591, 1220
- Kary, D. M., Lissauer, J. J., & Greenzweig, Y. 1993, *Icarus*, 106, 288
- Kinoshita, H., Yoshida, H., & Nakai, H. 1991, *Celestial Mechanics and Dynamical Astronomy*, 50, 59
- Kokubo, E., & Ida, S. 1998, *Icarus*, 131, 171
- Kominami, J., & Ida, S. 2002, *Icarus*, 157, 43
- Kominami, J., Tanaka, H., & Ida, S. 2005, *Icarus*, 178, 540
- Laskar, J. 1997, *Ast. & Astrophys.*, 317, L75
- Lecar, M., Podolak, M., Sasselov, D., & Chiang, E. 2006, *Ap. J.*, 640, 1115
- Lin, D. N. C., Bodenheimer, P., & Richardson, D. C. 1996, *Nature*, 380, 606
- Lisse, C. M., Beichman, C. A., Bryden, G., & Wyatt, M. C. 2007, *Ap. J.*, 658, 584
- Lovis, C., et al. 2006, *Nature*, 441, 305
- Masset, F. S., D'Angelo, G., & Kley, W. 2006, *Ap. J.*, 652, 730
- Masset, F. S., Morbidelli, A., Crida, A., & Ferreira, J. 2006b, *Ap. J.*, 642, 478
- McNeil, D., Duncan, M., & Levison, H. F. 2005, *AJ*, 130, 288
- McNeil, D. S., & Nelson, R. P. 2009, *Mon. Not. R. Astr. Soc.*, , 392, 537
- Morbidelli, A., Crida, A., Masset, F., & Nelson, R. P. 2008, *Ast. & Astrophys.*, 478, 92
- Nelson, R. P. 2005, *Ast. & Astrophys.*, 443, 1067
- Nelson, R. P., & Papaloizou, J. C. B. 2004, *Mon. Not. R. Astr. Soc.*, , 350, 849
- Paardekooper, S.-J., & Mellema, G. 2006, *Ast. & Astrophys.*, 459, L17
- Paardekooper, S.-J., & Mellema, G. 2008, *Ast. & Astrophys.*, 478, 245
- Paardekooper, S.-J., & Papaloizou, J. C. B. 2009, *Mon. Not. R. Astr. Soc.*, , 394, 2283
- Papaloizou, J. C. B., & Larwood, J. D. 2000, *Mon. Not. R. Astr. Soc.*, , 315, 823
- Papaloizou, J., & Lin, D. N. C. 1984, *Ap. J.*, 285, 818
- Papaloizou, J. C. B., & Szuszkiewicz, E. 2005, *Mon. Not. R. Astr. Soc.*, , 363, 153
- Papaloizou, J. C. B., & Terquem, C. 1999, *Ap. J.*, 521, 823
- Payne, M. J., Ford, E. B., Wyatt, M. C., & Booth, M. 2009, *Mon. Not. R. Astr. Soc.*, , 393, 1219
- Pollack, J. B., Hubickyj, O., Bodenheimer, P., Lissauer, J. J., Podolak, M., & Greenzweig, Y. 1996, *Icarus*, 124, 62
- Raymond, S. N., Barnes, R., & Mandell, A. M. 2008, *Mon. Not. R. Astr. Soc.*, , 384, 663
- Saha, P., & Tremaine, S. 1992, *AJ*, 104, 1633
- Shakura, N. I., & Sunyaev, R. A. 1973, *Ast. & Astrophys.*, 24, 337
- Tanaka, H., Takeuchi, T., & Ward, W. R. 2002, *Ap. J.*, 565, 1257
- Tanaka, H., & Ida, S. 1999, *Icarus*, 139, 350
- Tanaka, H., & Ward, W. R. 2004, *Ap. J.*, 602, 388
- Terquem, C., & Papaloizou, J. C. B. 2007, *Ap. J.*, 654, 1110
- Thommes, E. W., Duncan, M. J., & Levison, H. F. 2003, *Icarus*, 161, 431
- Thommes, E. W. 2005, *Ap. J.*, 626, 1033
- Thommes, E. W., Nilsson, L., & Murray, N. 2007, *Ap. J. Lett.*, 656, L25
- Torres, G., Winn, J. N., & Holman, M. J. 2008, *Ap. J.*, 677, 1324
- Ward, W. R. 1997, *Icarus*, 126, 261
- Wisdom, J., & Holman, M. 1991, *AJ*, 102, 1528
- Zhou, J.-L., Lin, D. N. C., & Sun, Y.-S. 2007, *Ap. J.*, 666, 423